Tampere University

Antti Tilja

X-RAY MICRO COMPUTED TOMOGRAPHY (µ-CT) IMAGE ENHANCEMENT WITH ARTIFICIAL INTELLIGENCE (AI)

Faculty of Information Technology
and Communication sciences
Master's Thesis
May 2022

ABSTRACT

Antti Tilja: X-RAY micro computed tomography image enhancement with artificial intelligence
Master's Thesis
Tampere University
MSc Electrical Engineering
May 2022

Micro computed tomography and X-ray imaging as a whole are commonly used imaging techniques in research and medicine. As artificial intelligence has become more and more commonly used over the years it has also proven its place in medical imaging. Machine learning is used in most fields of research and the development of deep learning has improved the efficiency of AI even more. AI has already made detecting diseases and making diagnoses easier and faster and in the future, there will be even more improvements in the field of medical technology due to artificial intelligence.

The purpose of this thesis was to examine how micro computed tomography images can be improved with artificial intelligence. Moreover, the image reconstructions were done with fewer projections than normally to see if image quality could be sustained with a lower projection count. Usually in CT imaging the projection count of reconstructions is around one thousand to acquire adequate image quality. The images used in this thesis were reconstructed with 1600, 800, 400, 200, and 100 projections. Dragonfly software was used for the AI. AI models were trained with different parameters to find out the best way to enhance image quality.

As an overall result it can be said that with proper training data, AI is a very viable tool for enhancing images. The best results were gained with 800 and 400 projection images. The results show that the network training data should be similar to the image enhanced and filtering the output data also helps improve image quality. 200 and 100 projection image quality could not be improved enough to have practical use. The images taken with different exposure times had so few detectable differences that there was nothing that could be concluded from them.

Keywords: micro-computed tomography, artificial intelligence, image quality

TIIVISTELMÄ

Antti Tilja: X-RAY micro computed tomography image enhancement with artificial intelligence
Diplomityö
Tampereen yliopisto
Sähkötekniikan DI-ohjelma
Toukokuu 2022

Mikro-tietokonetomografia, ja röntgenkuvantaminen ylipäänsä, ovat yleisesti käytettyjä kuvantamistapoja sekä tieteellisessä tutkimuksessa että lääketieteessä. Yksi suurimmista kehityssuunnista lääketieteellisessä kuvantamisessa nykyään on tekoälyn käyttö, joka on yleistynyt runsaasti viime vuosien aikana. Koneoppiminen on jo käytössä suurimmassa osassa tieteen aloista. Syväoppimisen kehitys ja suuremmat laskentatehot ovat mahdollistaneet entistä tehokkaampien tekoälyjen toteuttamisen. Tekoälyn avulla sairauksia pystytään jo havaitsemaan ja hoitamaan paremmin, ja tulevaisuudessa tekoälyllä tulee olemaan vielä suurempi rooli lääketieteen alalla ja diagnostiikassa.

Tämän opinnäytetyön tarkoitus oli tutkia tekoälyn kykyä parantaa mikro-tietokonetomografiakuvien laatua. Kuvat olivat rekonstruktioitu erilaisilla projektiomäärillä. Tämän tarkoitus oli tutkia, kuinka paljon pienemmillä projektiomäärillä rekonstruktioitujen kuvien laatua pystyy parantamaan. Yleensä tietokonetomografiassa käytetty projektiomäärä on noin 1000, jotta kuvanlaatu on riittävä. Tässä työssä käytetyt kuvat olivat rekonstruktioitu 1600, 800, 400, 200 ja 100 projektiolla. Tekoälyn opettamiseen käytettiin Dragonfly- tietokoneohjelmaa. Tekoälyjen opetuksessa käytettiin erilaisia neuroverkkorakenteita ja opetusdatoja, jotta paras mahdollinen vaihtoehto kuvien laadun parantamiseksi löytyisi.

Työstä saaduista tuloksista havaitaan, että pienemmillä projektiomäärillä rekonstruktioitujen kuvien laatua pystytään parantamaan huomattavasti. Parhaat tulokset saatiin kuvilla, jotka olivat rekonstruktioitu 800 ja 400 projektiolla. Tuloksista huomataan myös, että tekoälyn opetusdatan tulisi olla samankaltaista, kuin parannettavat kuvat. Lisäksi opetusdatan laadukkuus on suoraan verrannollinen tekoälyn kykyyn parantaa kuvia. Kuvien, jotka olivat rekonstruktioitu 200 ja 100 projektiolla, laatua ei pystynyt parantamaan tarpeeksi, jotta niillä olisi jokin käytännön tarkoitus.

Avainsanat: mikro-tietokonetomografia, tekoäly, kuvanlaatu

CONTENTS

LIST OF SYMBOLS AND ABBREVIATIONS

3-D	three dimensional
AI	Artificial Intelligence
ANN	Artificial Neural Network
CNR	Contrast-to-Noise ratio
CT	Computer Tomography
ROI	Region of Interest
SNR	Signal-to-Noise ratio
μ-CT	micro-Computed Tomography
e	electron
N	number of photons
h(x)	deconvolution kernel
p(x)	projection value
μ	mean
δ	standard deviation

1. INTRODUCTION

X-ray imaging and computed tomography are commonly used imaging techniques when it comes to research and medicine. Many X-ray techniques are based on samples ability to attenuate X-rays. Different materials and tissues have specific attenuation constants which gives them different colours in the X-ray images. This imaging method is called absorption imaging and it is also largely utilized in micro-computed tomography. The image quality of X-ray images can be very good, depending on the contrast differences. With bigger attenuation differences in materials, different regions can be seen clearly, but materials with low attenuation constants, such as soft tissues, it can be difficult to see certain structures. There are some ways to improve the attenuation of certain materials, for example contrast agents, but finding new solutions for better image quality is important. [1]

Artificial intelligence and machine learning have become widely used in scientific research and everyday life. As data can be gathered from almost anything, AI can be taught to perform various tasks. The development of deep learning has made AIs even more efficient and powerful. Also massive improvement in computing power have enabled more complex AI networks. With the help of deep learning, there has been big advances, for example in the field of computer vision, that would not have been possible with just machine learning. In CT imaging AI has been used to optimize and automate patient positioning, scan positioning, protocol selection, parameter selection, and image reconstruction, which has led to reduced patient radiation. [1]

In this study there will be given basic theoretical knowledge of X-ray and the operating principles of micro computed tomography. Image reconstruction is also discussed as well as the factors affecting image quality and noise. Artificial intelligence is handled by basics of machine learning and deep learning and commonly used network structures.

The aim of this study was to find out how micro-computed tomography image quality can be improved with the help of artificial intelligence. Tomographic micro-CT images reconstructed with different projection counts were used to train different AI networks to improve image quality. These networks were then used to enhance different micro-CT images to assess the image quality improvements and the usability of the images reconstructed with lower amounts of projection data.

2. X-RAY MICRO COMPUTED TOMOGRAPHY

Micro-computed tomography is an imaging method used examine the internal structures of tissue samples, materials, and even small animals. The resolution on µ-CT images is usually in the scale of micrometers. CT scanner has an X-ray tube, which acts as source for the X-rays, and a detector. A basic X-ray imaging system has been presented in figure 1. The imaging subject is placed between the source and the detector. In normal CT scan only the X-ray source and detector spin around the subject but in µ-CT the imaging subject can also be placed on base that spins. This spinning emotion enables scanning the subject from every angle to create a 3-D model. [2]

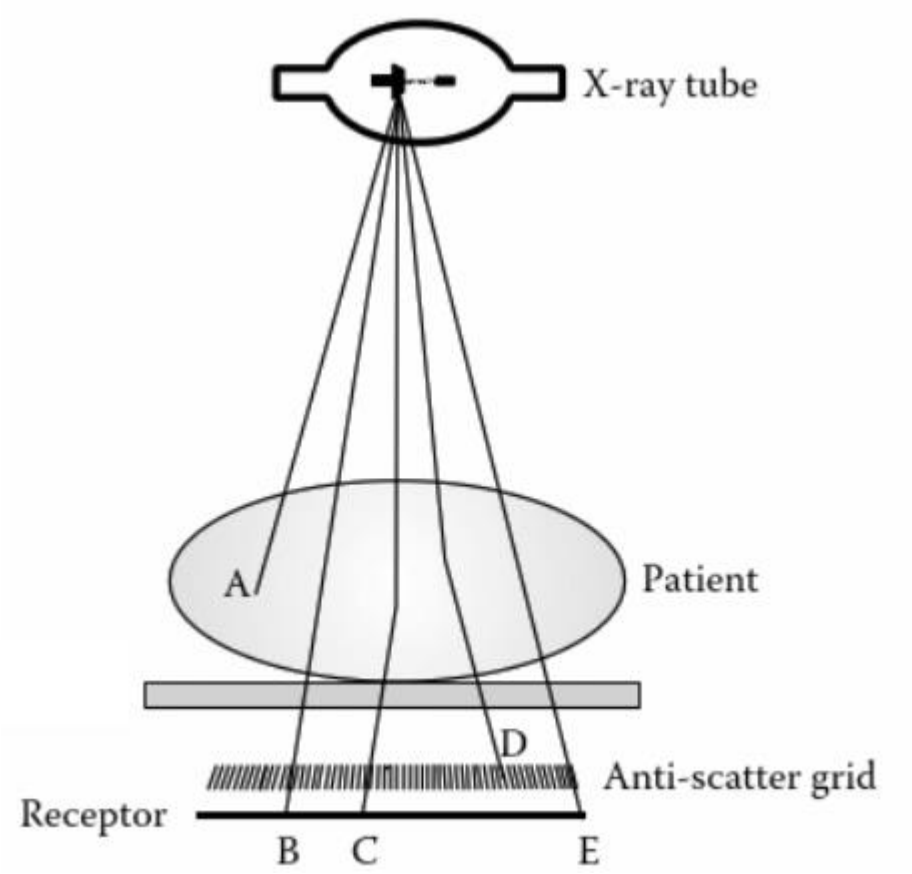

Figure 1. *A basic X-ray imaging system. A represent a photon that has been absorbed. B and E are photons that passed through patient without interacting with material. C and D are photons that have scattered. Modified from [3].*

2.1 X-ray

X-rays are a form of electromagnetic radiation with ionizing properties. X-ray has been widely used in medical imaging since X-ray imaging was discovered in 1895 by Wilhelm Röntgen. X-ray imaging, as CT and µ-CT, is based on the scattering and absorption of

X-ray photons and detecting the X-ray photons coming from the X-ray source to the detector through the imaging subject. [4]

The X-rays are produced by accelerating electrons with high voltage between a cathode and an anode. When electrons collide with the anode most of their energy turn into heat but some of the electrons decelerate in proximity of the atomic nuclei of the anode creating X-ray bremsstrahlung. The X-ray beam is then directed through the imaging subject to the detector where the photon intensities are observed. [4, 5]

The attenuation of the X-ray depends on the material properties of the subject. The main properties are thickness (x) and density (μ). With equation 1 the number of photons (N) passing through material can be calculated knowing the number of incident photons (N_0). The different interactions X-rays have going through the imaging subject are photoelectric effect, pair producing, and Rayleigh and Compton scattering. Due to the energy of the X-ray used in most medical imaging photoelectric effect and Compton scattering happen more commonly than pair producing and Rayleigh scattering. [4, 5]

$$N = N_0 e^{-\mu x} \tag{1}$$

2.2 Computed tomography

As opposed to traditional planar X-ray images CT can be used to acquire cross-sectional slices of the whole imaging subject and even 3-D models. This is beneficial when the imaging subject has overlaying structures which could not be seen with just X-ray imaging. Typically, a CT scanner (fig. 2) has a rotating gantry and a table for the imaging subject. The X-ray source and detectors are located in the gantry. The table is able to move through the gantry, so the imaging subject does not need to be disturbed halfway through the imaging process. A collimator can be used to shape the X-ray beam which in CT scanners are usually in a shape of a cone or fan. In the gantry, at the opposite side of the X-ray source, the detector or an array of detectors receives the X-rays that passed through the imaging subject. Before the detector there is a possibility to use grids to reduce the number of scattered photons. [4, 5]

Figure 2. *A typical clinical CT scanner [3].*

The operating principles of micro computed tomography are the same as computed tomography, but they have their own special features. The biggest difference between µ-CT and clinical CT is that the µ-CT is operated on much smaller scale with significantly increased resolution and smaller pixel size. CT can be used to examine bigger structures on human body, but µ-CT can be used to study the morphology of samples and materials. Due to its smaller size, µ-CT is commonly used in imaging materials or small animals. [2, 3, 5]

2.3 Image reconstruction

In µ-CT and CT the final tomographic image is reconstructed from a large number of projections taken from every angle around the imaging subject. Usually, the number of projections needed for a satisfactory CT image is around one thousand. The data from individual projections is transferred from the detector to a computer. From the projections the computer reconstructs a 3-D model formed of cross-sectional slices. Usually, the projection data undergoes some modification before it can be used for reconstruction. To reduce noise low signal areas can be smoothened with the help of algorithms that

detect those areas. Also scatter correction and interpolation to fix dead pixels can be applied. [2, 3]

There are several different algorithms that can be used for the reconstruction of the projection data. Commonly used methods for reconstruction are Fourier-based reconstruction, iterative reconstruction, backprojection, and filtered backprojection. As the computing power has increased considerably over the years iterative reconstruction is becoming a better option than filtered backprojection which has been the most used method for CT reconstruction. [4, 5]

The backprojection method is based on calculating the attenuation coefficients of all the matrix pixels from the projection data. The value obtained from the projection data is placed in every pixel in the trajectory. Using several projections to acquire data improves the reconstructions accuracy. However, the radial blur still remains in the reconstruction. This can be corrected with the filtered backprojection which uses convolution to deconvolute the blur. Convolution is calculated with equation 2, where p(x) is the old projection value, p'(x) is the new projection value and h(x) is the deconvolution kernel, which is selected depending on the radial blur. A better-quality reconstruction can then be made from the deconvoluted projections. In the Fourier-based reconstruction the convolution is implemented with a Fourier transform. [3, 4, 5]

$$p'(x) = \int_{-\infty}^{\infty} p(x)h(x - x')dx' \coloneqq p(x) \otimes h(x) \qquad (2)$$

The iterative reconstruction method (fig. 3) can be used to acquire more accurate reconstruction with the same amount of projection data or same quality with less projection data than other methods. The algorithm uses an initial guess which is an image that is used to calculate iterations. The algorithm then uses those iteration to update the image. Values from the measured image are compared to the iterated images generated values. By calculating the difference between the generated projection values and the real projection values and error matrix is generated. The error matrix updates with every iteration to minimize the error values. Finally, the algorithm forms a tomographic image with better accuracy. [3, 4, 5]

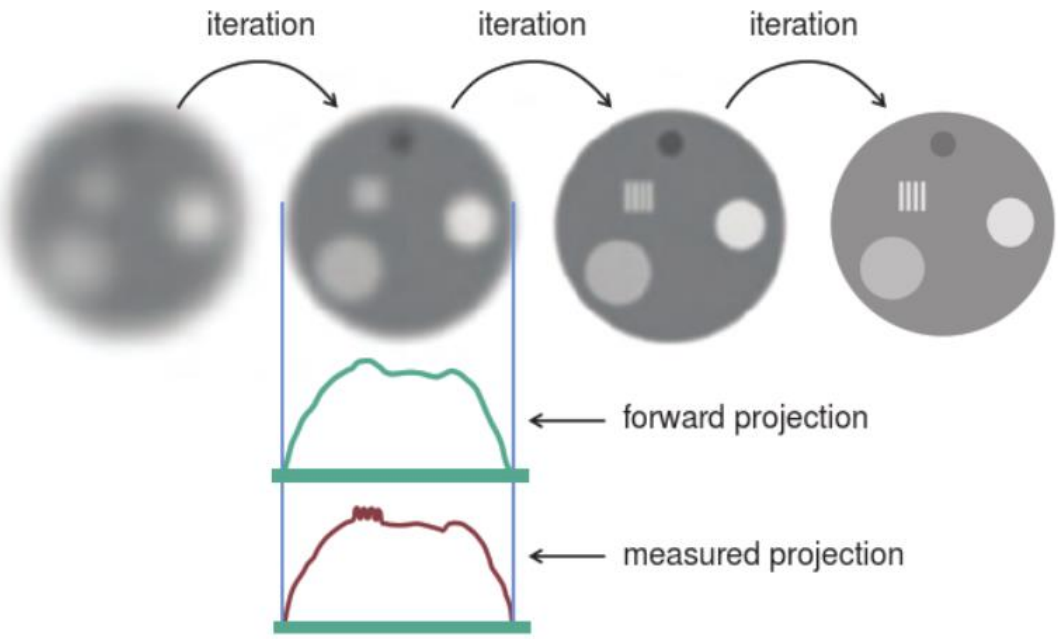

Figure 3. *The iterative reconstruct method. An Initial guess is used to compute a forward projection, which is then compared to the measured data to create an error matrix. [4]*

2.4 Image quality

Image quality can be adjusted with various methods depending on the information that needs to be seen from the image. Some of the things that most affect the image quality are the imaging subject, radiation dose, and X-ray source and detector. In medical imaging contrast and spatial resolution are important image characteristics for image quality. [4, 6]

2.4.1 Contrast resolution

The contrast of an image is defined by the difference of the intensity values in the image. In imaging with X-ray, the contrast is due to attenuation differences. A higher contrast resolution is required to detect smaller changes of intensity values and structures with similar composition. The contrast of an image is composed of two components: detector and subject contrast. Detector contrast is dependent on physical properties of the X-ray detector. Subject contrast is gained from the X-ray after it has passed through the imaging subject which is why it has more variables that have an effect to its value. These variables can be divided into external and internal factors. External factors include the characteristics of X-ray source and produced radiation. Internal factors are due to attenuation of the radiation in different structures of the imaging subject. [4, 7]

The contrast resolution in CT imaging is also determined by reconstruction method, slice thickness and radiation exposure time. As mentioned in chapter 2.3. the iterative reconstruct method can produce better-quality images with less noise and higher contrast resolution. Using thicker slices for reconstruction will lower the noise level due to higher amount of X-rays used to acquire the data.[4]

One efficient way to increase contrast is to use contrast agents to enhance the absorption of the X-rays in specific tissue types. This is especially effective when imaging soft tissue. A lot of information can be lost in soft tissue imaging without the use of contrast agents due to poor attenuation contrast of soft tissues. Specific tissues can be labeled with a contrast agent that has high effective atomic number to enhance the contrast of the tissue. Typical contrast agents used in medical imaging are iodine and barium. [4, 6, 7]

For a quantitative analysis of image quality some calculations can be made. Contrast-to-noise ratio (CNR) is used to evaluate the relative contrast difference between two regions of interest (ROI) and signal-to-noise ratio (SNR) is used to evaluate the amount of noise compared to signal. CNR can be calculated with equation 3, where μ_1 and μ_2 are the mean intensities of different ROIs and δ_2 is the standard deviation of the intensity of the second ROI. SNR can be calculated with equation 4, where δ_{sample} is the standard deviation of the intensity of the sample and $\delta_{background}$ is the standard deviation of the intensity of the background which is due to the noise in the image. [2, 6, 7, 8]

$$CNR = \frac{\mu_1 - \mu_2}{\delta_2} \quad (3)$$

$$SNR = \frac{\delta_{sample}}{\delta_{background}} \quad (4)$$

2.4.2 Spatial resolution

Spatial resolution expresses the amount of detail that can be distinguished from the image. Spatial resolution is mainly limited by the imaging equipment and the pixel size of the detector. In CT imaging also the reconstruction algorithms, and motion of the gantry and the imaging subject affect to the spatial resolution. To measure the spatial resolution properties there are few functions such as edge spread, and line spread which relate to the response of the imaging system for sharp edge or a line source. In medical imaging the spatial resolution is evaluated regularly by performing a line pair measurement. The relation between spatial resolution and contrast resolution is demonstrated in figure 4. Resolution and contrast in the diagrams decrease as noise increases. [4, 6]

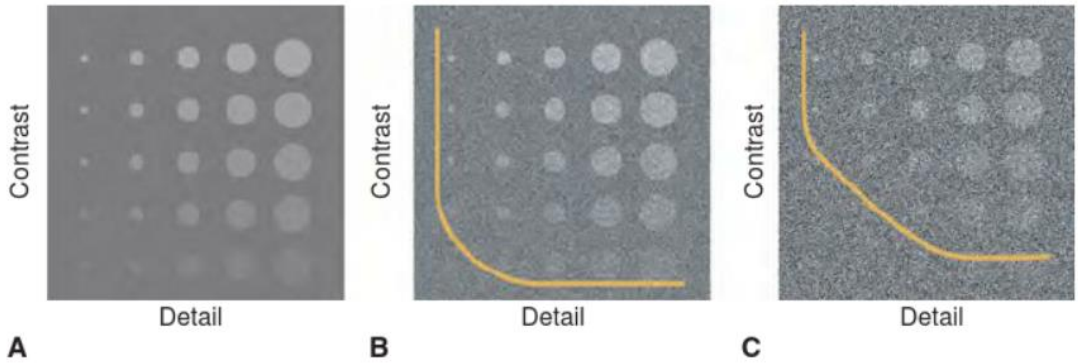

Figure 4. *Contrast-detail diagrams. In diagram A there is no noise present. As the noise level increases in diagrams B and C more disks become undetectable. The yellow line demarcates this disk that can and cannot be seen. [4]*

2.5 Noise

Noise affects the quality of all medical imaging. Noise is generated from many sources and cannot be entirely removed from the picture though some sources of noise are easy to avoid like using grids to prevent scattered X-rays going to detector. As in all electronic systems, CT scanners are exposed to electronic noise. With low signal levels electric noise can have a large impact on the image quality, for example in soft tissues where details are hard to distinguish without the help of contrast agents. Electronic noise is also caused by the structured noise coming from the detector. As the detector pixel data is acquired via amplifier circuits, the difference of the amplifier parameters causes structured noise. This noise can however be corrected because it is constant. [4, 6]

Another source of noise is anatomical noise. They are caused by the structures that are outside of the examined area. Subtraction imaging can be used to reduce anatomical noise. In CT imaging overlapping structures are easily separated so anatomical noise can be heavily reduced.[4]

3. ARTIFICIAL INTELLIGENCE

Artificial intelligence has become a widespread technology over the years. Artificial intelligence can be used to conduct feats previously thought to be impossible, for example digital assistants or self-driving cars. The number of applications for the use of AI is growing exponentially as it is applied to more and more everyday appliances. Artificial intelligence has almost become mandatory for many industries due to automation, data analysing capabilities, and achieving higher accuracy. [9, 10]

Artificial intelligence is based on intelligent behaviour of several artefacts. This includes operations related to learning, reasoning, acting, and perception in complex environments. Artificial intelligence has been developed to succeed in these tasks better and faster than the human brain is capable of. Though, a machine achieving the intelligence of a human still seems impossible, the field of artificial intelligence has had some outstanding breakthroughs. [9, 10]

The use of AI is changing the world fast, but the limits of artificial intelligence must be recognized before it can be fully utilized. AI networks, much like a brain, learn from data, which sets the limits to how much, how fast, and how accurately AI can perform different tasks. With more training data and time AIs become better and better. At present most AI systems are created to perform one specific task. This is one of the most significant downsides in developing artificial intelligence. [9, 10]

Artificial intelligence, and especially deep learning, has proved to be an essential part in the development on the field of medical imaging. In the past years AI and the medical applications it provides have generated considerable amount of interest. Deep learning techniques can be used to detect and identify risk factors and diseases from radiographic images, for example detecting tuberculosis or melanoma. These kind of advances make medical diagnosis easier to perform. AI can also be used to process and enhance image data to automate and facilitate the acquisition of better quality images. [11, 12]

Though AI has had substantial improvements that have resulted in great advances in the field of medical imaging there are some challenges with using artificial intelligence. Currently a major challenge to an extensive adoption of AI is the requirement of data for training the artificial intelligence networks. A lot of diverse data is needed, and it needs to be organized in order to be used effectively. Also finding the optimal network models and training methods for different implementations is something that needs further research. In the future these problems will be solved since AI has been proven to obtain

information that humans are not able to, and the demand for more efficient medical care is constant. [11, 12]

3.1 Machine learning

Machine learning is the basic method when implementing AI technology. Machine learning is a mix of statistical methods and computer science. In machine learning computers actions can adapt or alter to gain better accuracy depending on how well adjustments correlate on the actual results. This is done by algorithms trained with raw data to gain network models with desired features. With enough raw data and training these machine learning models can become intelligent enough to acquire results from data that has not been tested. [9, 10, 13]

3.1.1 Supervised learning

Supervised learning is a method of machine learning that in addition to the learning data uses the corresponding labels. This way it is ensured to have the data relate to its correct class. The training data consists of raw input data and also the data of desired output results. The function model can be simply described with equation 5,

$$y_i = a + Bx_i \tag{5}$$

where y_i is the target result, x_i is the input data, a is the intercept of y, B is the input feature, and i is iterated from 1 to N. [9]

Supervised learning contains a few different ways it can be implemented. Labelled and unlabelled data can be used simultaneously for training. This method is called semi-supervised learning. Data can also be fed from a dynamic environment to the algorithm as a positive or negative feedback. This method is called reinforcement learning and can be used for example autonomous cars when driving on a specific route. [9]

From machine learning techniques, supervised learning is the most extensively used. It has been used in many computer game AIs, where the computer learns from previously played games and becomes more intelligent. Supervised learning is also commonly used method in statistic, for example the k-nearest neighbours algorithm. Some other supervised learning examples are support vector machines, Markov models, and Bayesian networks, to name a few. [9, 10]

Another widely used supervised learning model in modern field of machine learning is support vector machine. Support vector machines take two multidimensional datasets and finds the ideal hyperplane between those two clusters. The model discovers marginal lines that are adequately separate for not one data point to exist between those

marginals and finds a direction for the discovered margins to be as wide as they can be. [9, 13]

3.1.2 Unsupervised learning

In unsupervised learning, the training data does not contain labels, but instead has hidden structures and patterns. From the input data the algorithm tries to detect underlying relations and resemblances to create a model. When the desired outputs for the data are unknown, it is more difficult to build models. Therefore, similarities in input data are gathered in separate clusters. Unsupervised learning algorithms can utilize dimensionality reduction, intrinsic patterns, feature learning, and outlier detection. Unsupervised learning can also be used in neural computing, for example adaptive resonance theory and self-organizing maps. [9, 10]

One commonly used unsupervised learning method is k-means clustering. The k-means clustering algorithm first defines the k. The test data is then randomly split to k clusters. In each cluster, the values of the data points are set to mean of the cluster. The data values are put on to clusters with the means nearest to the value. The algorithm updates the means and clusters all the data. Then it restarts and clusters the data again until the mean values are not changing anymore. [9, 10]

3.2 Deep learning

For decades, machine learning has been the main field of AI when building models. Previously building models has required a lot of knowledge in computation, statistical methods, and data and gaining access to this knowledge was not so easy. The availability of required knowledge has improved considerably, and ever more powerful machine learning models can be made with help of programming and statistical modelling. Deep learning is a field of AI under machine learning. It can be used to build more complex AI models. Deep learning uses neural networks and optimisation to create automated ways of detecting patterns and designs from data. The neural structure of deep learning networks allows the use of many different algorithms that together can make decisions on its own. Deep learning also needs more data for training than machine learning. [9, 10, 14]

At present, there are a few different AI libraries, for example TensorFlow, which can make building models faster and easier than before. The libraries have made access to data and network implementations significantly effortless and with help on deep learning many technologies have developed tremendously in the past years. There are many neural network structures to choose from and they all have uses in different places. The

most used network structures are convolutional neural network and recursive neural network. [9, 10, 14]

3.2.1 Neural networks

Neural networks are computing or biological systems that work like neurons or artificial nodes. They consist of layers of nodes, with inputs and outputs on the other sides. Neural networks are also called black box models due to the nonlinear multilayer structures from which it is very difficult to gain any information about the approximated function. Neural networks in computing have to be trained with data in order to make any estimations of further data and to function as an AI. The learning process for neural networks can be either supervised or unsupervised depending on if the output data is specified. [15]

3.2.2 Artificial neural networks

With inspirations from the biological neural networks, artificial neural networks are the brain-like structures commonly used in the field of AI. Artificial neural networks learn progressively with the minimizations of the cost function. The neuron layers in the network have varying number of nodes with different transformation functions and amplitudes that are applied to the inputs. Each of the neurons can send an output of a nonlinear function depending on the inputs. [15, 16, 17]

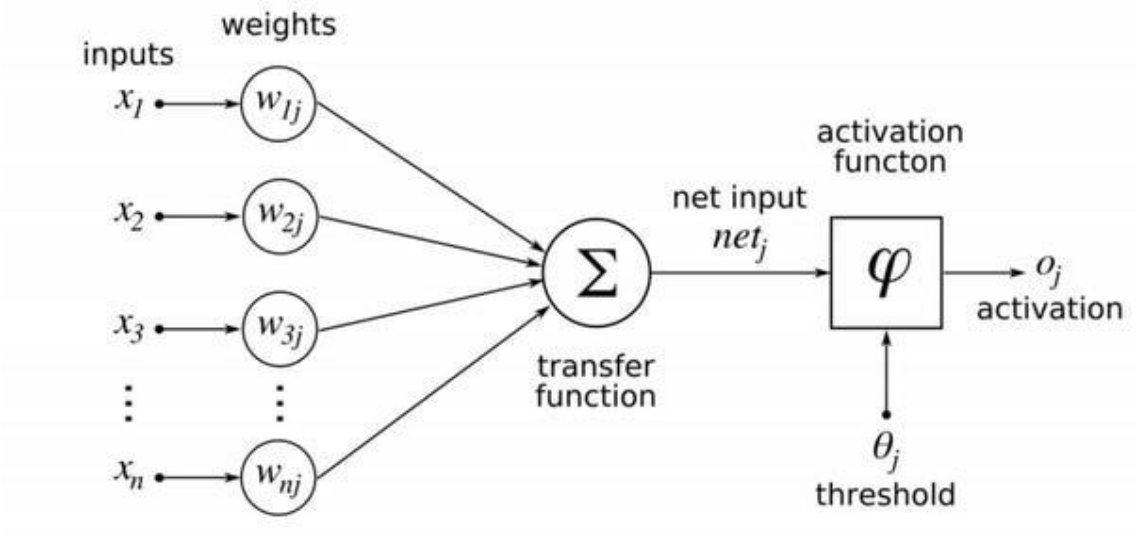

Figure 5. *A neuron model structure in artificial neural network. [18]*

The nonlinear functions are partly weighted (fig. 5) in the network and modulated in iteration. Layer by layer the weights of the neurons are adjusted with each iterations. The

iterations continue until the weighting is optimized. Artificial neural networks are regularly used with computer vision or speech recognition. [17]

3.2.3 Feedforward neural network

Feedforward neural network is a commonly used type of artificial neural network. The processes and recall patterns advance from one layer to the following layer as is seen in figure 6. There is no looping or backwards progression which is why it is called a feedforward network. The lack of reverse connection in the network distinguishes it from recurrent neural networks. [15, 19]

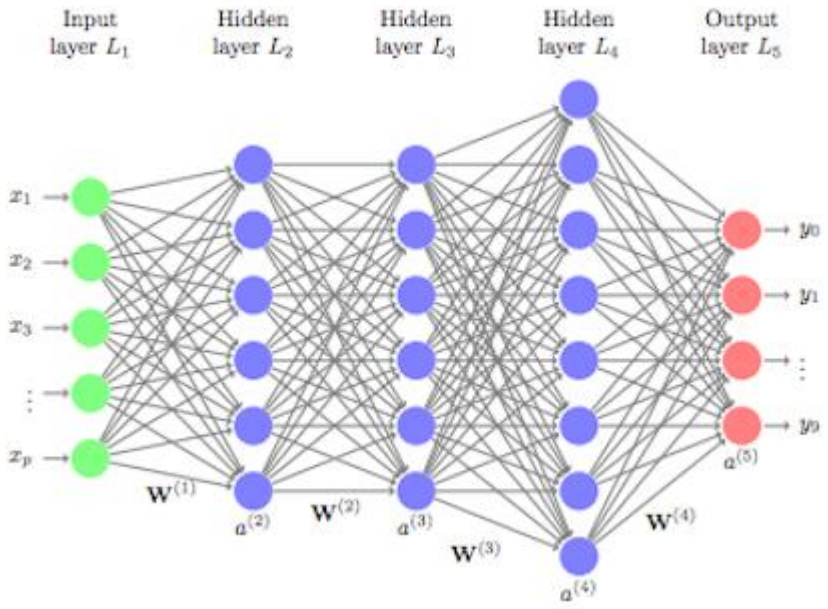

Figure 6. *A feedforward neural network with input, output, and three hidden layers. [20]*

3.2.4 Recurrent neural network

Recurrent neural networks are very similar to feedforward neural networks with exception of layers being able to form backwards connections or loops. One difficulty with loops in recurrent neural networks is that the loop might become endless if the stopping conditions are not taught to the network. This can be avoided by using context neurons, computing output over a limited number of iterations, or computing output up until the network output stabilizes. [15, 16, 19]

Recurrent neural networks, like other networks, learn by training with raw data. In comparison to feedforward networks, recurrent networks can also use previously generated output as an input to produce more output values in the network. [16]

3.2.5 Convolutional neural network

Convolutional neural network is a neural network that uses convolution in some of its layers instead of matrix multiplication. Convolutional neural networks can learn high-order features from data, which makes them very effective to use in image recognition and computer vision. It is also largely used in voice data processing, text analysis, and robotics. Convolutional neural networks are best trained and used with data with spatial correlation and some visible structure. [21]

In comparison to other neural networks convolutional neural networks have a better structure for processing image data. In convolutional neural network the input image data is transformed into output sets of class probabilities through many connected layers. Neurons in neural layers can form three-dimensional structures, with specific height, length, and depth. These structural attributes make it possible to process image such as pixel height and width, and the RGB channels data more efficiently. [21]

3.2.6 Recursive neural network

Recursive neural networks function on the recursive nature of many objects for example sentences and images. The inputs of the network are reconstructed and as a result classified based on what kind of content is found. Recursive neural networks have a binary tree structure where every parent maps two children recursively and each node is given a score. This kind of structure is great for parsing up scenes from images or sentences. Recursive neural networks can be applied using forward or backpropagation whether the input is at the bottom or the top of the binary tree. [22]

The two main variants of recursive neural networks are recursive neural tensor networks and recursive autoencoders. Recursive autoencoders use a semi-supervised learning method which means that there is a small quantity of labelled data. The network is taught to reconstruct the input and break it into segments. This method is commonly used in natural language processing. Recursive neural tensor networks utilize supervised learning and calculates vectors for the nodes in the binary tree structure. This network architecture is great for labelling and segmenting image objects. [23]

3.2.7 Autoencoder

Autoencoder is a neural network structure mostly used to learn compressed representations from datasets. The algorithm uses dimensionality reduction where the input data is reproduced with fewer dimensions. Autoencoder networks output layer has a target value which is the same value that the input layer has. This means that the number of neurons

in the input layer and output layer are the same. Autoencoders are best used with unsupervised learning and unlabelled data. [24]

Autoencoder networks have two main variations: compression autoencoder and denoising autoencoder. Compression autoencoders have a narrow hidden layer before the output is expanded back to the input size. Denoising autoencoders inputs have noise or some of their features are removed. The denoising autoencoder network learns to denoise the output. [24]

4. MATERIALS AND METHODS

The aim of this study is to examine the use of artificial intelligence to enhance µ-CT image quality. The work process of this thesis is seen figure 7.

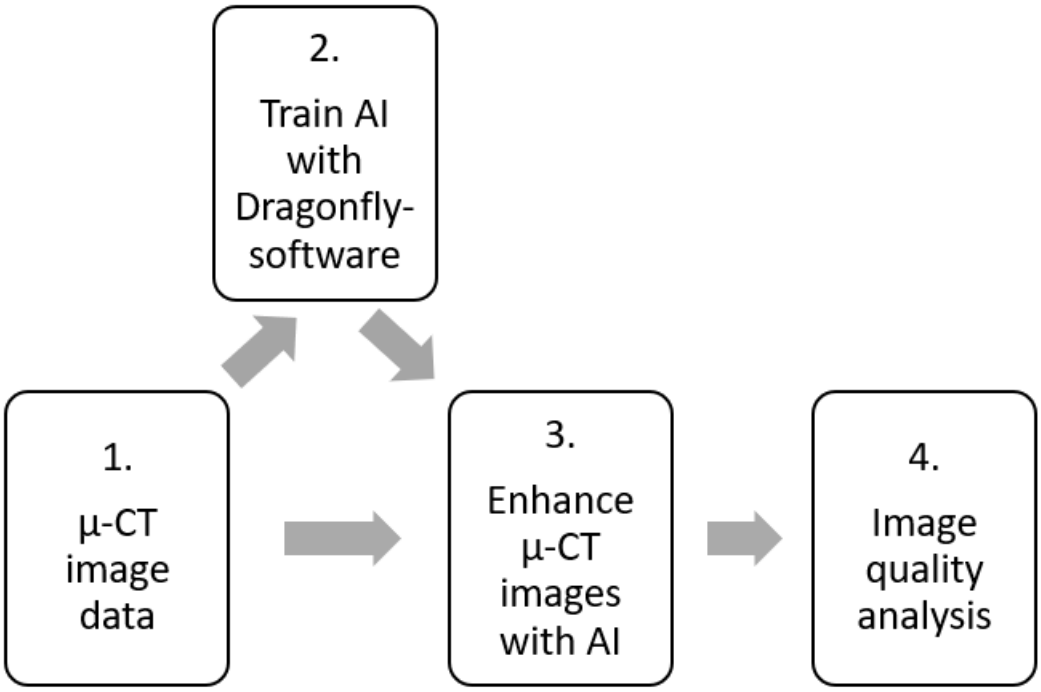

Figure 7. *Process of work in the thesis.*

The images are taken from three different samples of biomaterial which are named after their structure: particles, particles and pores, pores and fibers. There is also one biological sample which is a pig's eye. The images were taken with Zeiss Xradia MicroXCT-400, which is a high resolution 3D X-ray imaging system optimized for imaging complex internal structures. Software for the AI was Dragonfly 2020.1 by Object Research Systems. The Dragonfly software is designed for 3D visualization and analysis. All of the images and results presented were gained by using Dragonfly.

4.1 Images

For training data of the AI models the images were reconstructed with different number of projections varying from 3200 to 100 depending on the sample. 1600 projection was used for reference as it is considered to be of standard quality. Particles and pores-sample also has a corrected version of the 1600 projection reconstruction, which had better quality than the uncorrected version. The pores and fibers- sample was imaged

using absorption and phase imaging with varying exposure time, which affected the number of photons on the detector. A full list of images used can be found in table 1 and images of different reconstructions of each sample can be found in appendix A.

Table 1. List of all the images used in training AI networks and assessing their quality enhancing capabilities.

Sample	Voxel size (µm)	Imaging technique	Number of projections	Number of photons (only for pores and fibers)
Particles	5,63	Absorption	100 200 400 800 1600	
Particles and pores	2,28	Absorption	200 400 800 1600 1600	
Pig eye	28,20	Absorption	200 400 800 1600	
Pores and fibers	5,64	Phase contrast	1600 1600 1600	400 3000 6000
		Absorption	1600 1600 1600 1600 3200	1800 3500 7000 14000 5000

4.2 AI models

For the model architecture, there were three different options for denoising found in the software: Auto-Encoder, Noise2Noise, and U-Net. Noise2Noise and U-Net are convolutional networks. Each of these were used. The network training was done with different amounts of slices varying from 1 to 11 which was the maximum amount. Data augmentation and validation were used. A full list of AI models trained is found in appendix B. The AI models were also numbered to simplify referring to them in later parts.

4.3 Analysis methods

To evaluate the AI's ability to enhance the images a total of five different analysis were conducted. The first analysis was to examine which of the three available architectures was able to produce the best quality images. The second analysis was to find out how the quality of the network training input data affects the quality of the images. The third analysis was to examine the effect of the network training output data quality on the

quality of the images. The fourth analysis was how AI network trained with data from different sample than the sample analysed affects the quality of the images. The fifth analysis was to examine the effects of exposure time and the number of photons on detector on image quality, and how the AI can enhance the images with lower exposure time. All of these analyses were applied to images with different reconstruction projection count to also see how much different reconstructions can be enhanced.

All the image slices enhanced were no used in training of the networks and they were also mirrored on the x-axis. Before any analyses were done the intensity values of the images were normalized to scale from 0 to 255. All numerical values were obtained using the histogram tool in Dragonfly. SNR values were calculated for each of the analyses using equation 4. How the sample and background area were defined for each sample can be found in appendix C. Since there were no specific structures that were examined as the picture quality was inspected as a whole the sample area was chosen to be the entire image. A relative change for the SNR values was also calculated in some cases using equation 6, where x is the calculated SNR value of an enhanced image and $x_{reference}$ is the SNR value of the original image.

$$Relative\ \ change = \frac{x - x_{reference}}{x_{reference}} \tag{6}$$

A line intensity analysis was also conducted in some cases. A line was drawn onto the image and intensity values of pixels under the line were used to draw a graph. This method was used to see the changes in amount of detail of the images. The placement of the line in each of the pictures is also found in appendix C. The lines were placed so there would be different structures to see how the sharpness of borders is affected.

4.3.1 Architecture

The three different architectures available were U-Net, Noise2Noise and Autoencoder. Using these architectures, convolutional neural networks can be created. In this first part the most suitable architecture for CT image enhancement was examined.

Three networks were trained for this, one for each type of architecture. Image data used was the particles dataset. Input slice count was set to one. Input projection count was 200 and output projection count was 1600. The images enhanced were the 100, 200, 400, and 800 projection reconstructions from the particles dataset.

4.3.2 Input data quality

The input data quality testing was conducted by training networks with different input projection count. Also different input slice counts were used. In this second part the amount of data needed for network training in order to give usable results was tested.

A total of 18 networks were trained for this part. Image dataset used was the particles dataset. Networks were trained with input projection counts of 200, 400, and 800. Output projection count was 1600. For each input projection count networks with input slice counts of 1, 3, 5, 7, 9, and 11 were trained. The images enhanced were the 100, 200, 400, and 800 projection reconstructions from the particles dataset.

4.3.3 Output data quality

For the output data quality assessment, networks were trained with different output image data. The purpose of this part was to examine if it is worthwhile to enhance the training data before training the network.

The dataset used for this part was particles and pores. Input projection count was 200 and output projection count was 1600. Two different networks were trained with original and corrected output data. Input slice count was set to one. The images enhanced were 200, 400, and 800 projection reconstructions from the particles and pores dataset.

4.3.4 Training with different sample

In this fourth part images enhanced with networks trained with the same dataset as the image and another dataset were tested. This way the necessity to have similar images for training the networks as the images enhanced can be found out.

The datasets used for network training were particles and pig eye. Both datasets were used to train three networks. Input projection counts for the networks were 200, 400, and 800. Output projection count was 1600. Input slice count was 11. The images enhanced were 200, 400, and 800 projection reconstructions from the pig eye dataset.

4.3.5 Photon count and exposure time

The fifth test was done by using images taken with different exposure times as inputs for networks. Also the images used for output data had different exposure times. This way it possible to see what kind of improvement in image quality can be achieved with lower radiation exposure times and thus photon counts.

The dataset for network training in this part was pores and fibers with two different kinds of images taken with absorption contrast imaging and phase contrast imaging. A total of

five networks were trained. Input and output data had varying photon counts from 400 to 14000. More detailed information about the data used in training of each network is found in appendix B. The input slice count was set to 11. The projection count for the images was 1600 except for one which had a projection count of 3200. As the normal micro-CT images have a photon count at least 5000 for adequate image quality, only the images with lower photon count were enhanced.

5. RESULTS

5.1 Architecture

The SNR calculations for the model architecture comparison are found in table 2. The SNR value for the original 1600-projection reconstruction was 7,49. The line intensity profiles of the different image enhancements are found in appendix D. In these graphs, images of the same reconstruction with use of different AI model to enhance them are compared to 1600-projection reconstruction. The U-Net architecture gave the best results, so it was used in the later parts of the thesis.

Table 2. The SNR calculations of the model architecture comparison. Image name refers to the sample and the projection count used for the reconstruction of the image. The AI model number refers to the number presented in appendix B.

SNR					
Architecture	AI model number	Image			
		Particles 100	Particles 200	Particles 400	Particles 800
Original image		1,95	4,21	4,58	6,24
Auto-Encoder	1	2,61	7,29	13,08	14,87
Noise2Noise	2	1,99	7,19	12,62	13,66
U-Net	4	2,03	9,00	13,67	15,54

Figures 8, 9, and 10 are example images of the 400-projection reconstruction. The images are enhanced with the three network models used in this part. Figure 11 is the original 1600-projection reconstruction for comparison.

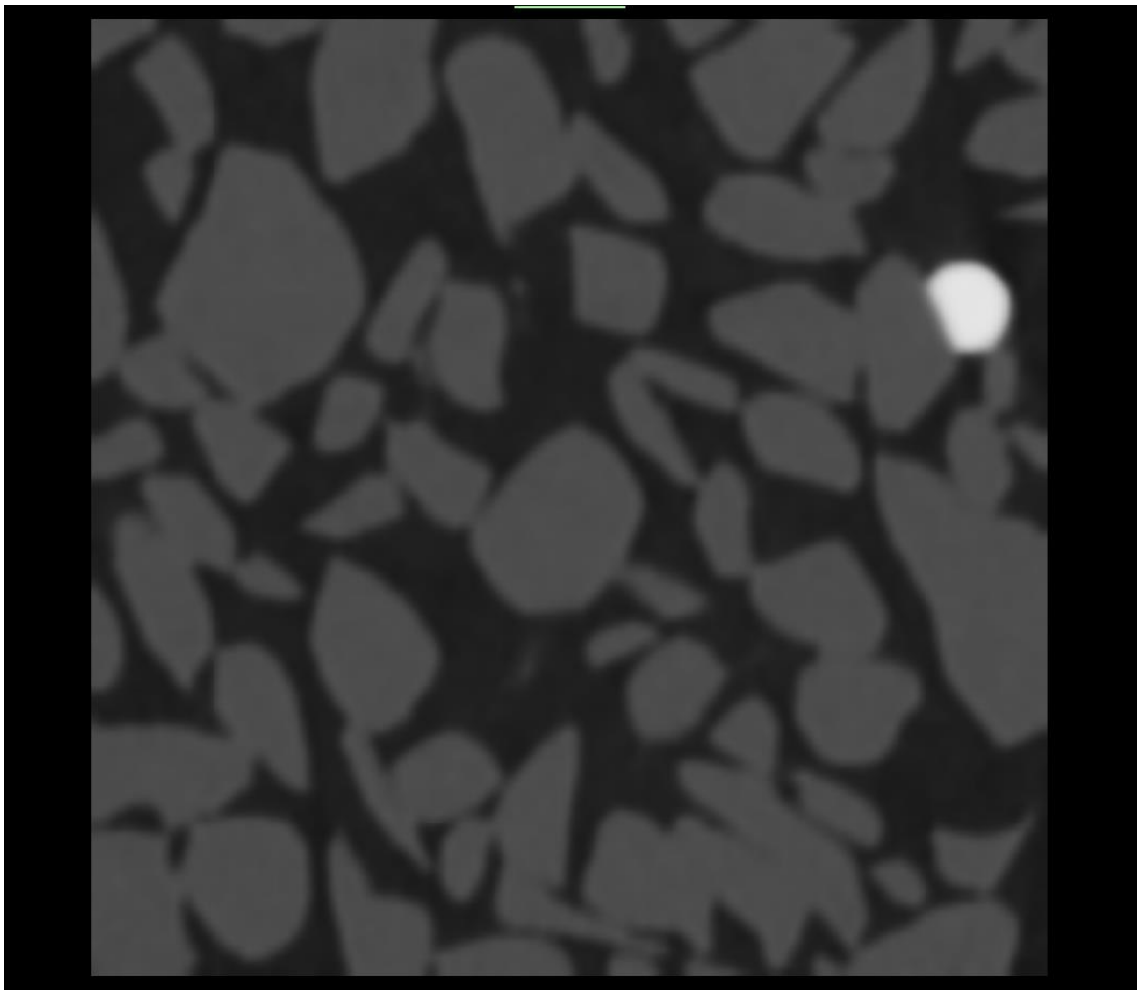

Figure 8. *400-projection reconstruction of particles dataset enhanced with AI model number 1.*

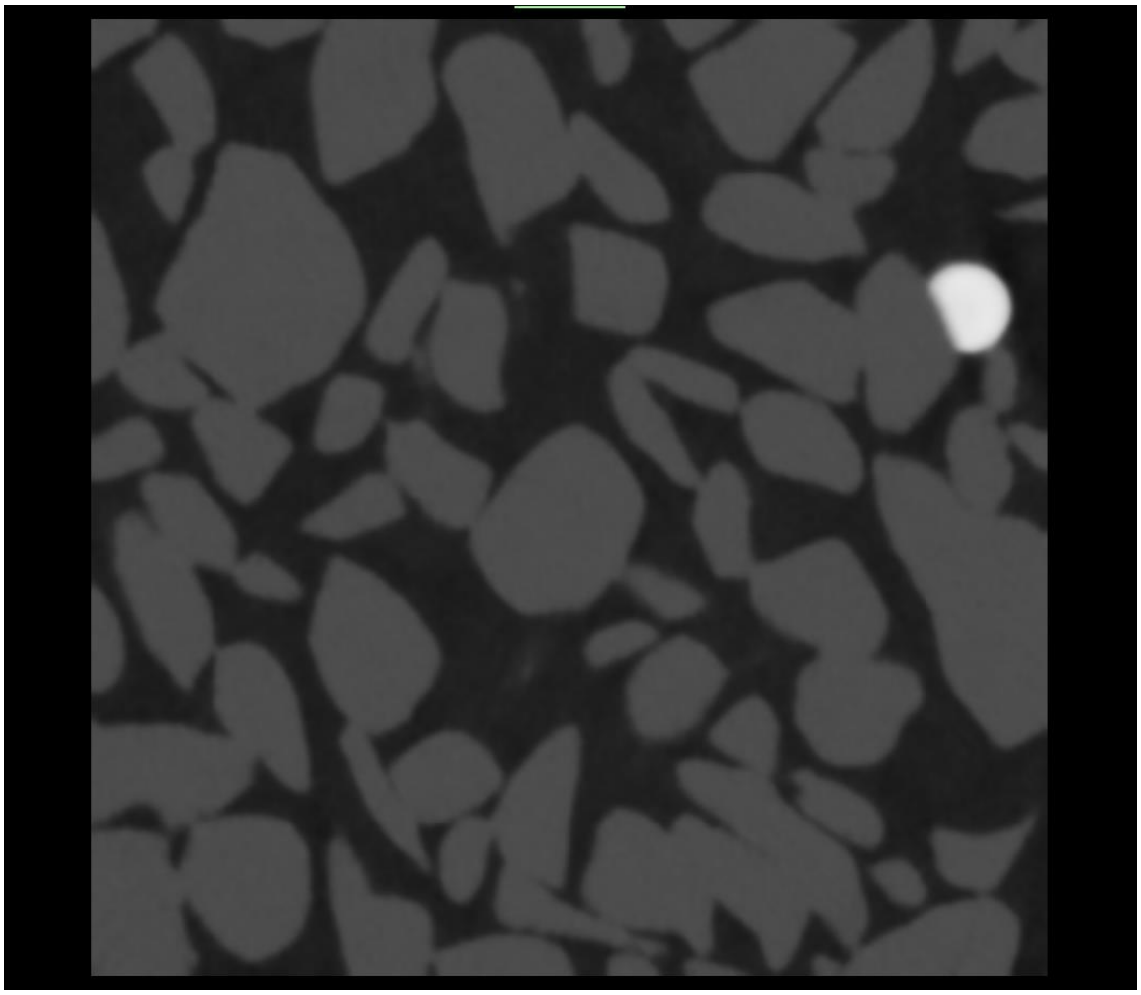

Figure 9. *400-projection reconstruction of particles dataset enhanced with AI model number 2.*

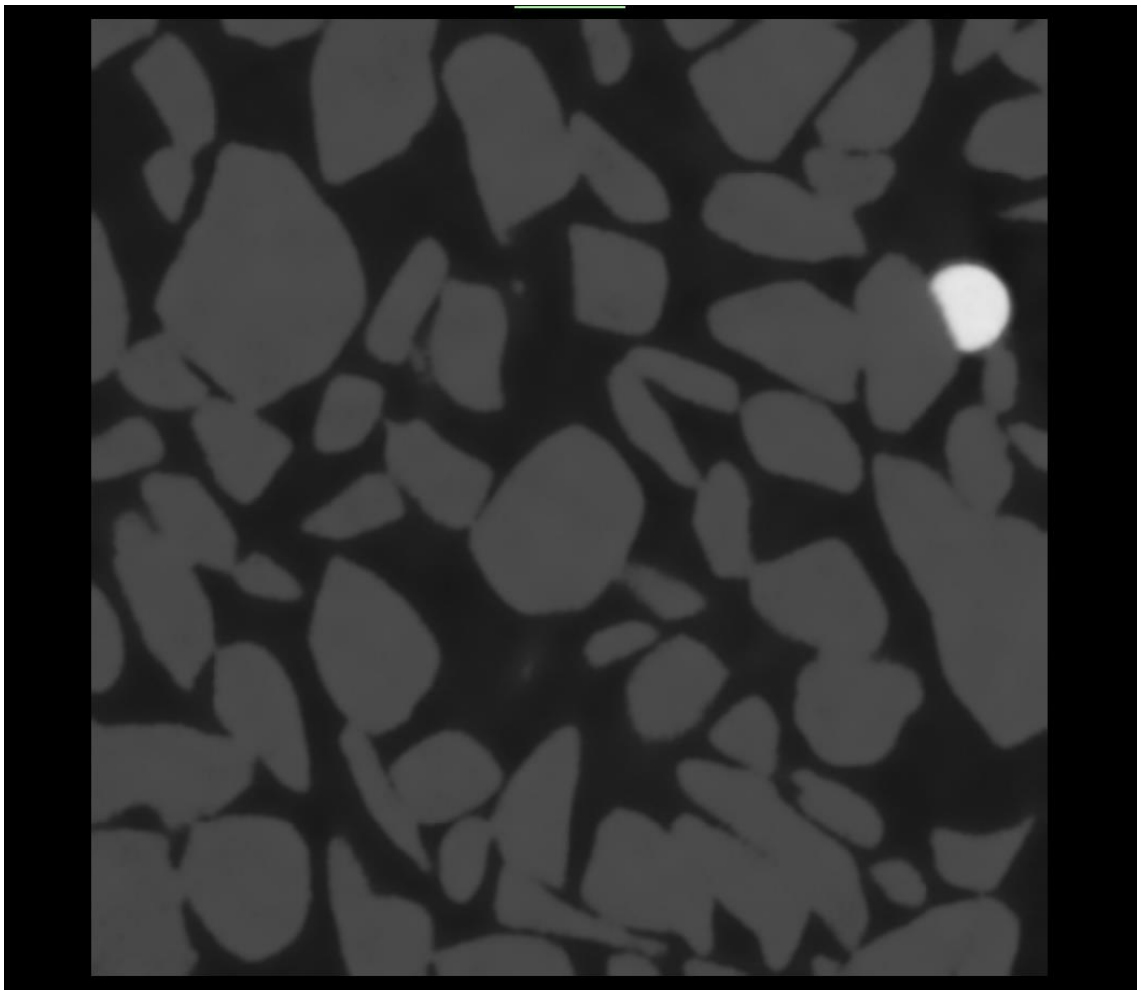

Figure 10. *400-projection reconstruction of particles dataset enhanced with AI model number 3.*

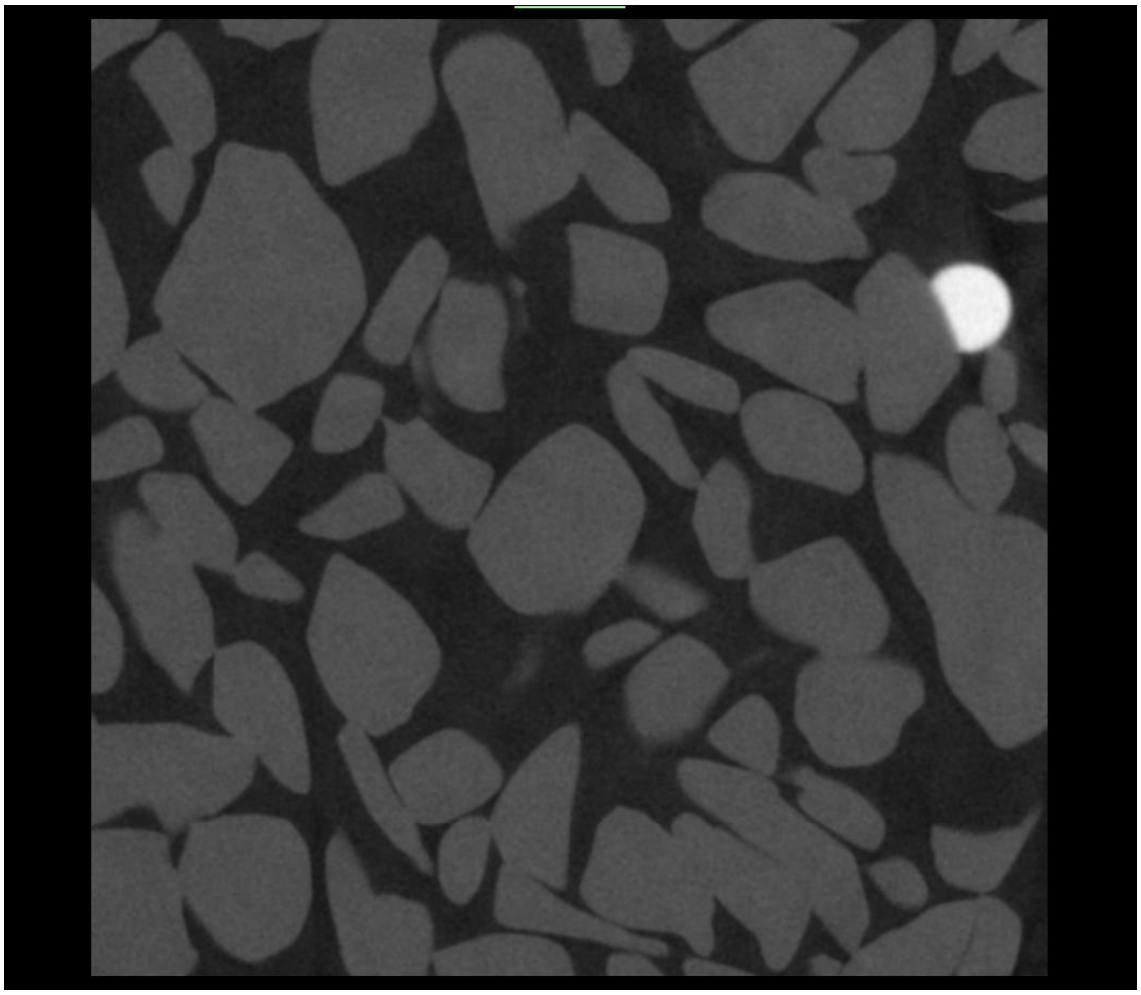

Figure 11. *1600-projection reconstruction of particles dataset.*

5.2 Input data quality

The SNR calculations for the network training input data quality analysis are found in table 3. For better comprehension of the SNR values relative changes were also calculated and they are found in table 4.

Table 3. The SNR calculations of the network training data input quality analysis. AI model number refers to the numbers presented in appendix B. The image name refers to the sample and the projection count of the reconstruction.

SNR					
Input projection count	AI model number	Image			
		Particles 100	Particles 200	Particles 400	Particles 800
Original image		1,95	4,21	4,58	6,24
200	4	2,03	9,00	13,67	15,54
200	5	1,96	10,81	12,27	12,91
200	6	1,89	11,91	12,45	14,43
200	7	1,73	11,51	13,31	15,85
200	8	1,86	10,96	11,71	12,49
200	9	1,77	11,83	13,42	13,98
400	10	2,06	4,49	9,35	11,30
400	11	1,96	4,69	9,05	10,78
400	12	2,02	4,68	9,39	11,26
400	13	2,06	4,99	9,91	11,38
400	14	1,88	4,98	9,89	10,79
400	15	1,92	4,88	10,01	11,01
800	16	2,08	3,37	6,32	8,51
800	17	2,02	3,58	6,86	8,74
800	18	2,09	3,44	6,53	8,69
800	19	2,08	3,51	6,80	8,94
800	20	1,94	3,48	6,87	8,75
800	21	1,97	3,45	6,75	8,78

Table 4. The SNR relative change calculations of the network training data input quality analysis. AI model number refers to the numbers presented in appendix B. The image name refers to the sample and the projection count of the reconstruction.

SNR relative change (%)					
Input projection count	AI model number	Image			
		Particles 100	Particles 200	Particles 400	Particles 800
200	4	4,10	113,78	198,47	149,04
200	5	0,51	156,77	167,90	106,89
200	6	-3,08	182,90	171,83	131,25
200	7	-11,28	173,40	190,61	154,01
200	8	-4,62	160,33	155,68	100,16
200	9	-9,23	181,00	193,01	124,04
400	10	5,64	6,65	104,15	81,09
400	11	0,51	11,40	97,60	72,76
400	12	3,59	11,16	105,02	80,45
400	13	5,64	18,53	116,38	82,37
400	14	-3,59	18,29	115,94	72,92
400	15	-1,54	15,91	118,56	76,44
800	16	6,67	-19,95	37,99	36,38
800	17	3,59	-14,96	49,78	40,06
800	18	7,18	-18,29	42,58	39,26
800	19	6,67	-16,63	48,47	43,27
800	20	-0,51	-17,34	50,00	40,22
800	21	1,03	-18,05	47,38	40,71

Figures 12, 13, 14, and 15 are example images of the 100, 200, 400, and 800 projection reconstructions. The images are enhanced with AI model number 10. Figure 16 is the original 1600-projection reconstruction for comparison.

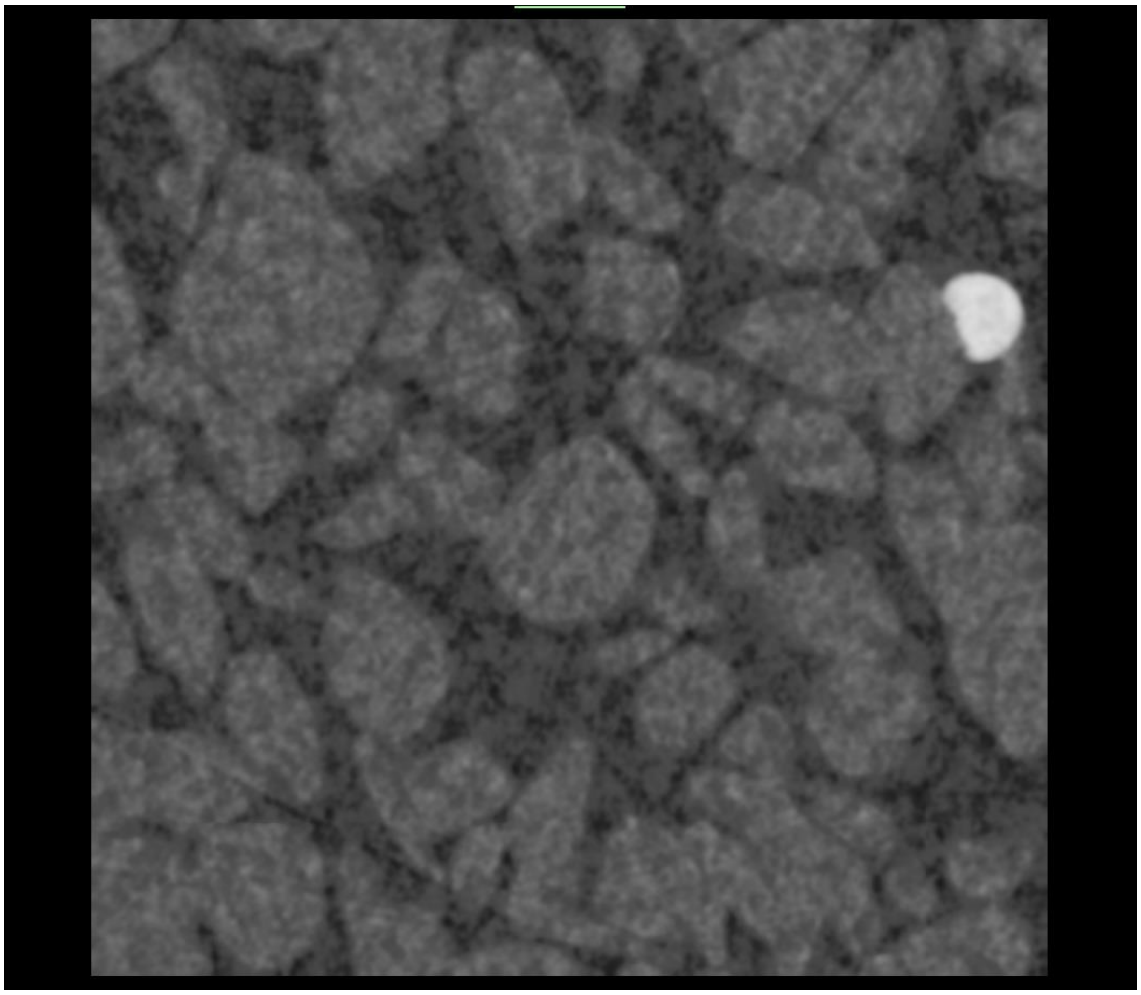

Figure 12. *100-projection reconstruction of particles dataset enhanced with AI model number 10.*

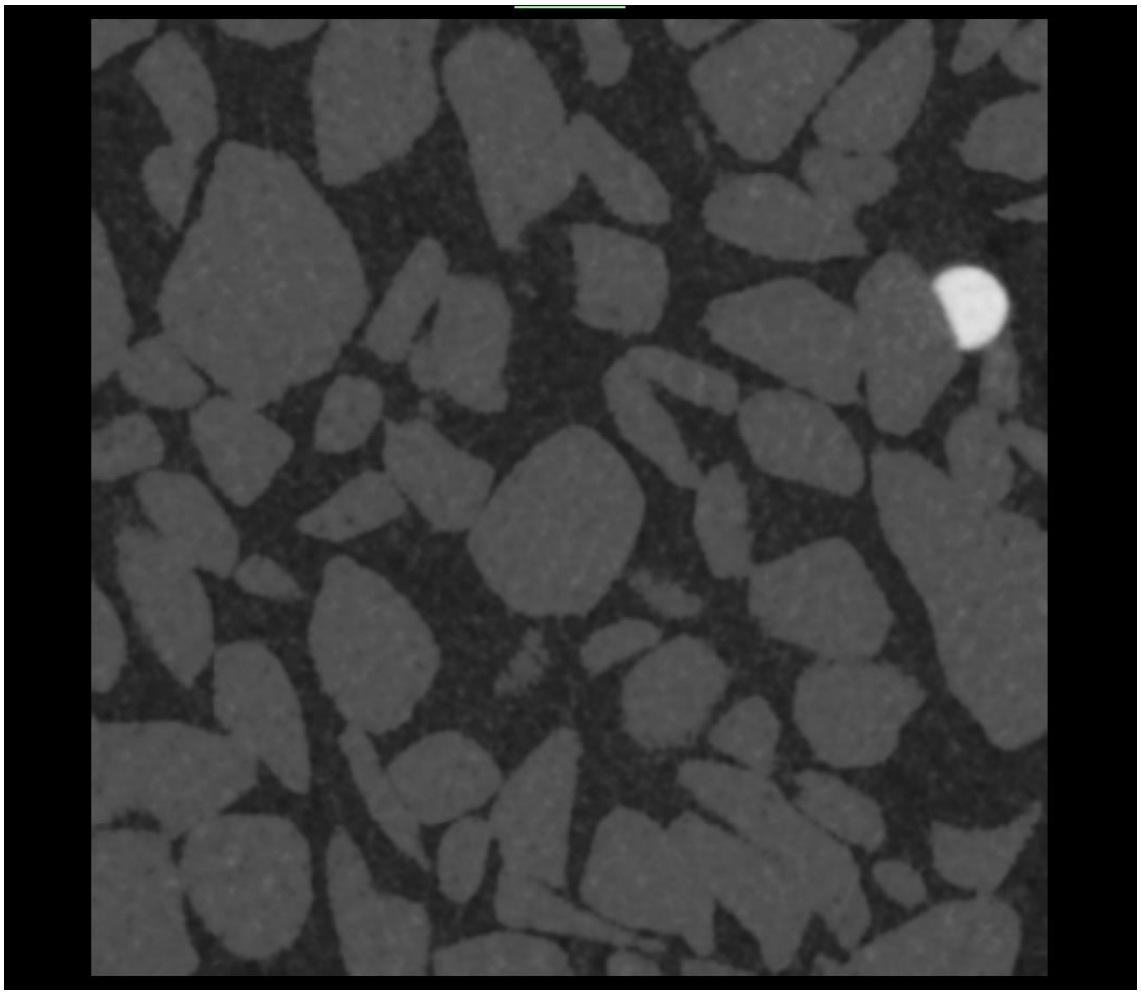

Figure 13. *200-projection reconstruction of particles dataset enhanced with AI model number 10.*

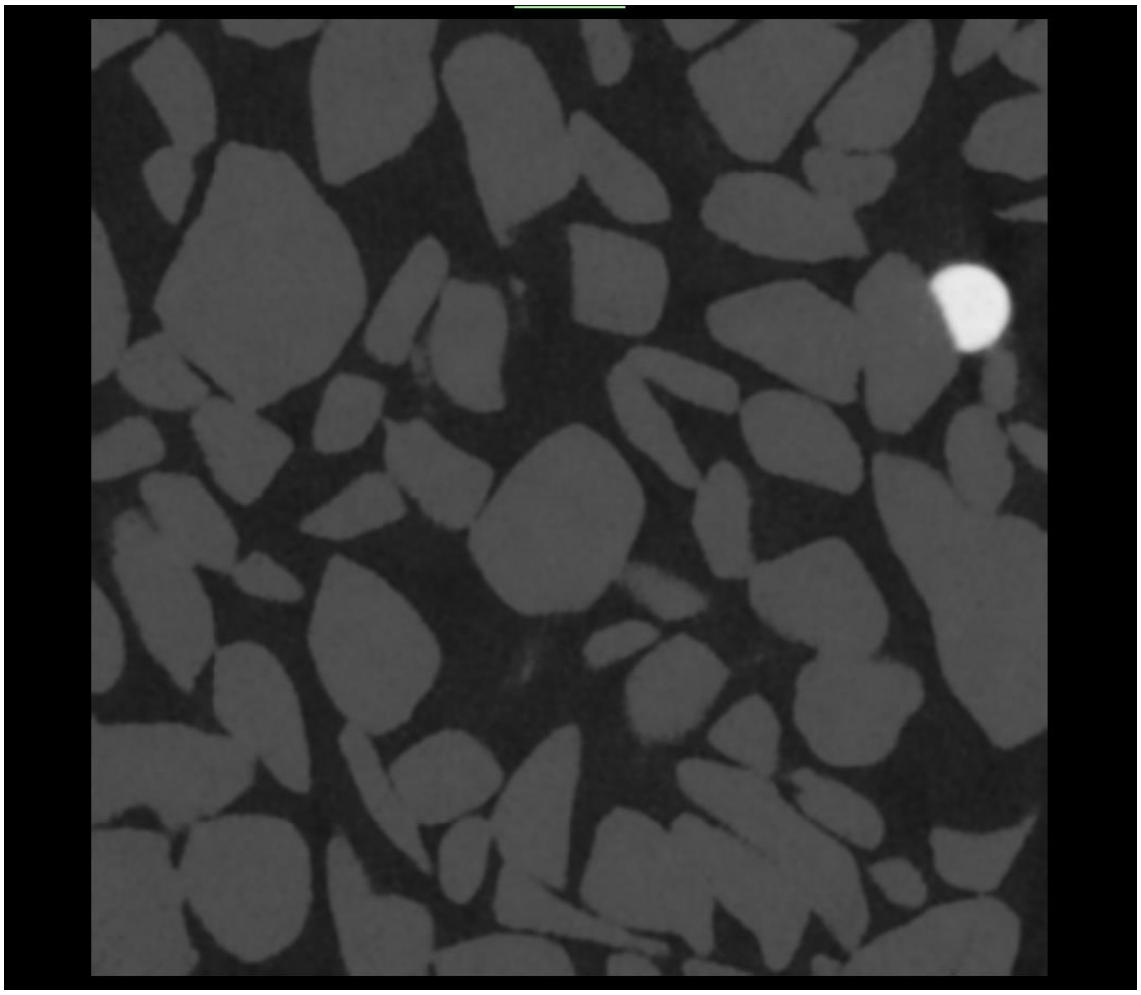

Figure 14. *400-projection reconstruction of particles dataset enhanced with AI model number 10.*

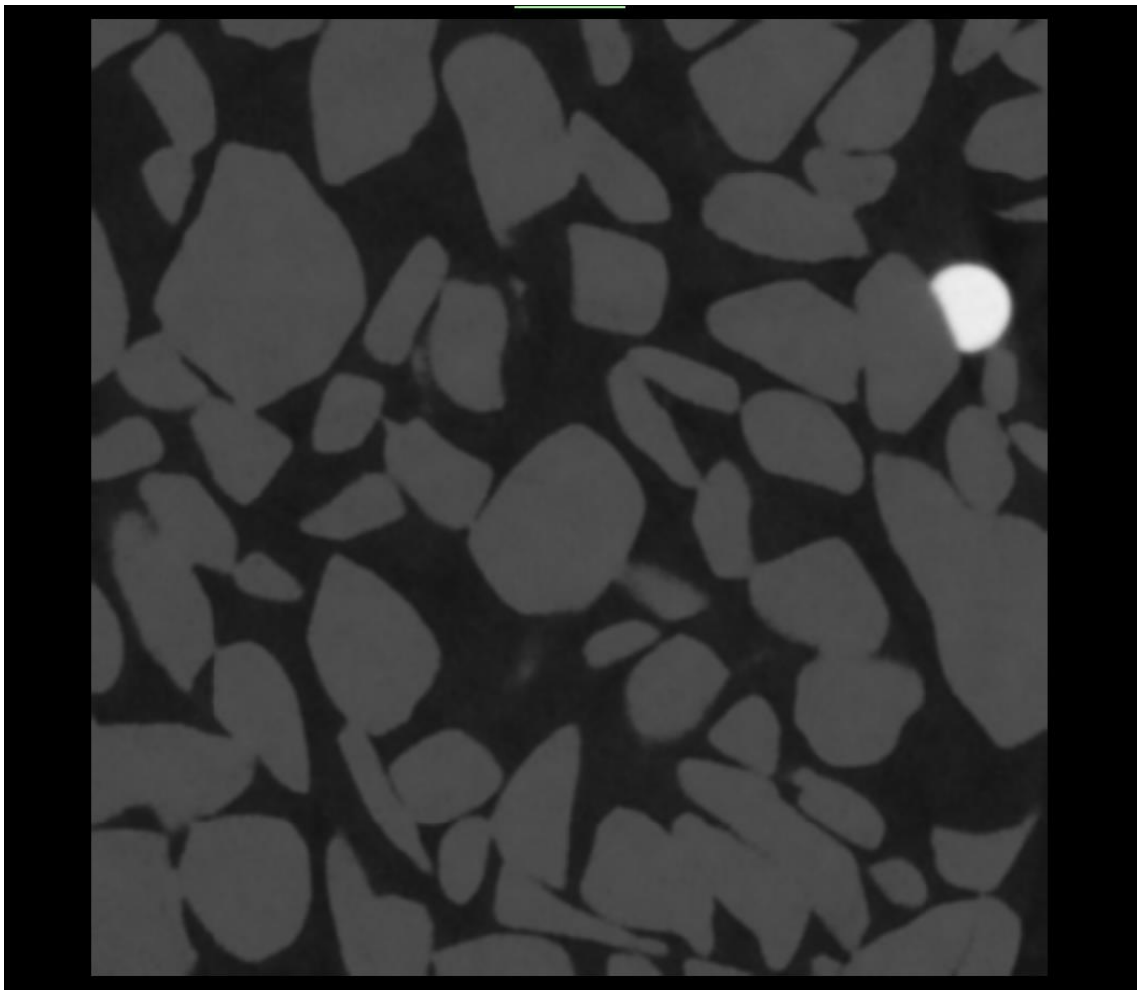

Figure 15. *800-projection reconstruction of particles dataset enhanced with AI model number 10.*

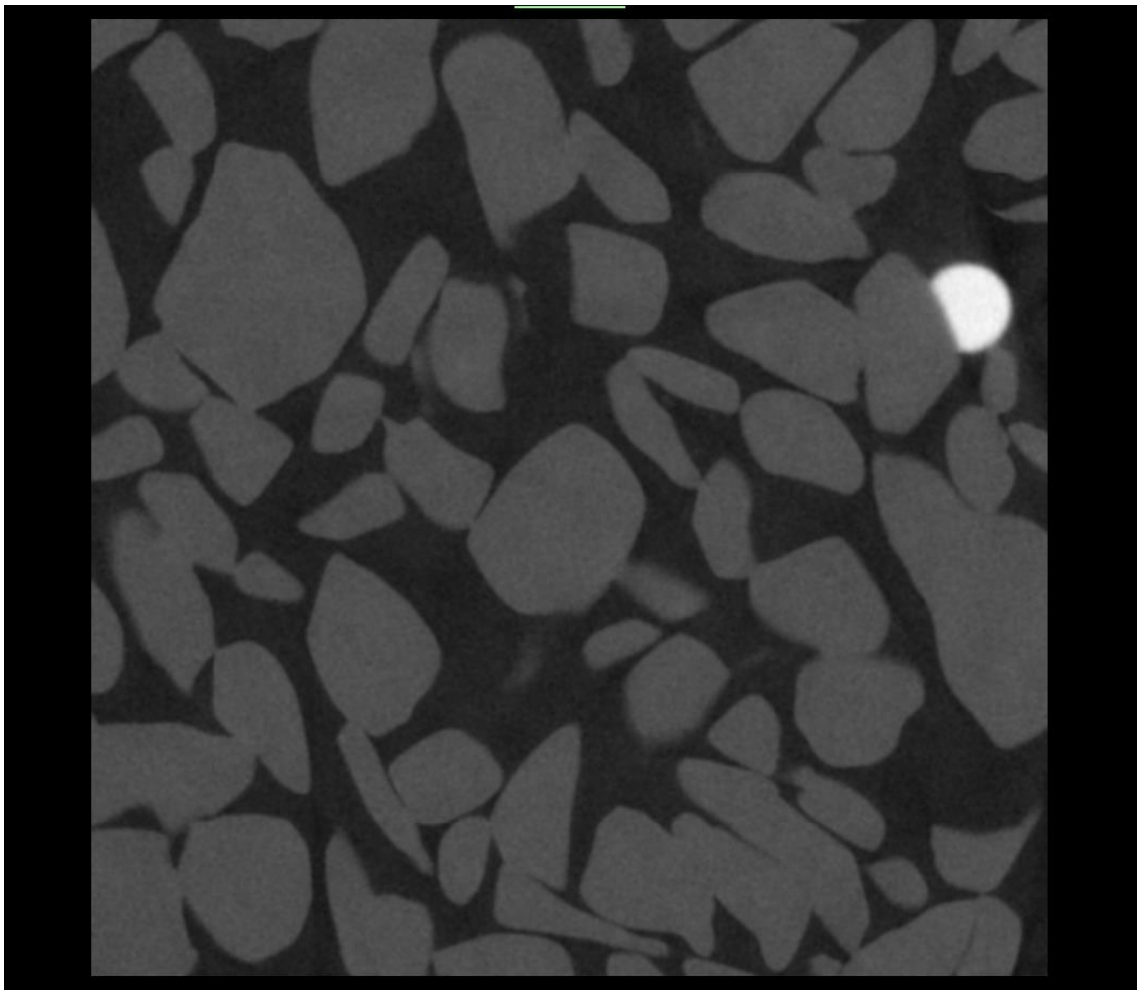

Figure 16. *1600-projection reconstruction of particles dataset.*

5.3 Output data quality

The SNR calculations for the network training output data quality analysis are found in table 5. The line intensity profiles of the different image enhancements are found in appendix E.

Table 5. The SNR calculations of the network training data output quality analysis. AI model number refers to the numbers presented in appendix B. The image name refers to the sample and the projection count of the reconstruction.

		SNR				
Output data	AI model number	Image				
		Particles and pores 200	Particles and pores 400	Particles and pores 800	Particles and pores 1600	Particles and pores 1600 (corrected)
Original image		3,15	4,02	4,32	4,24	11,89
Original	22	4,57	4,59	4,58	-	-
Corrected	23	15,71	16,21	15,85	-	-

In figures 17 – 22 are the images enhanced in this part. The images are enhanced with both AI models used in this part. Figures 23 and 24 are the original 1600-projection reconstructions for comparison.

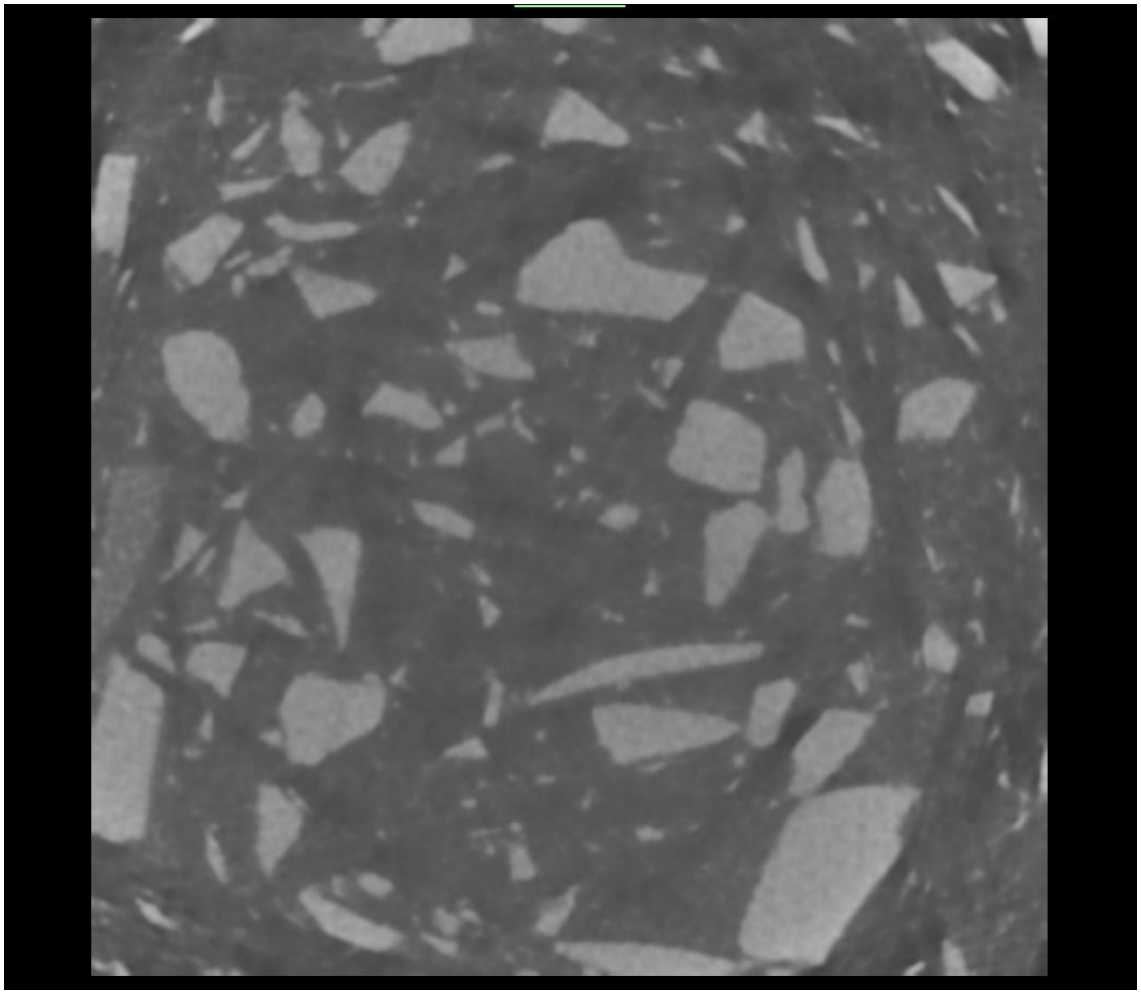

Figure 17. *200-projection reconstruction of particles and pores dataset enhanced with AI model number 22.*

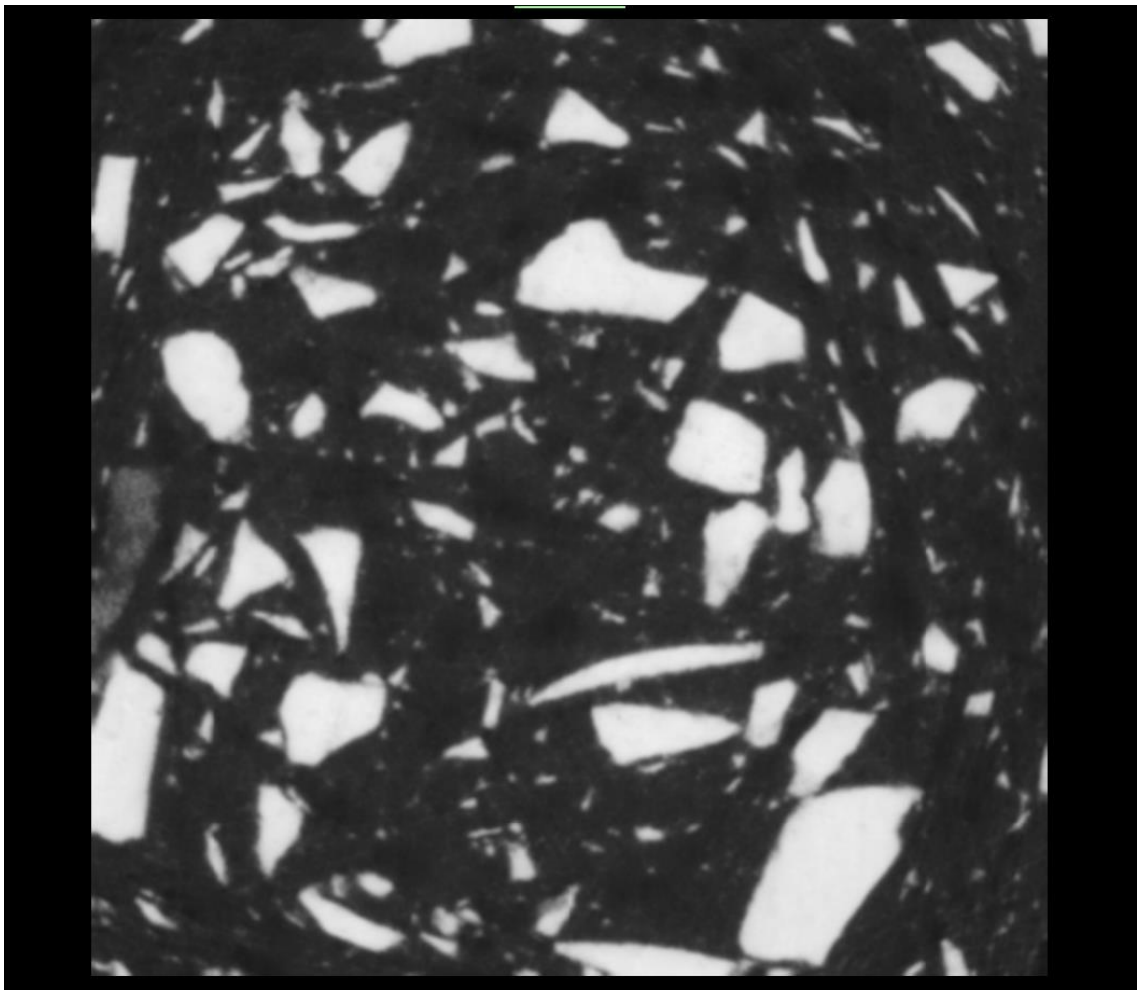

Figure 18. *200-projection reconstruction of particles and pores dataset enhanced with AI model number 23.*

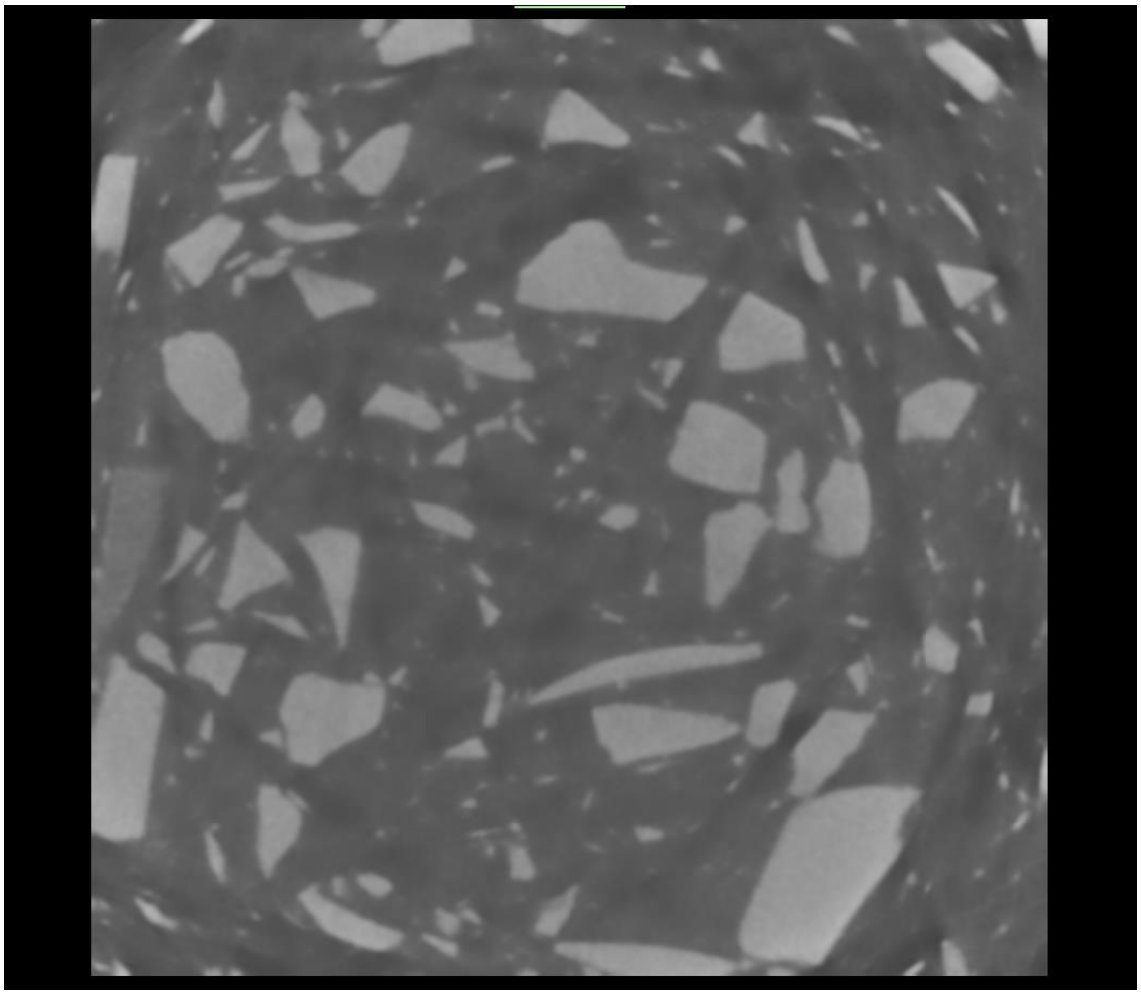

Figure 19. *400-projection reconstruction of particles and pores dataset enhanced with AI model number 22.*

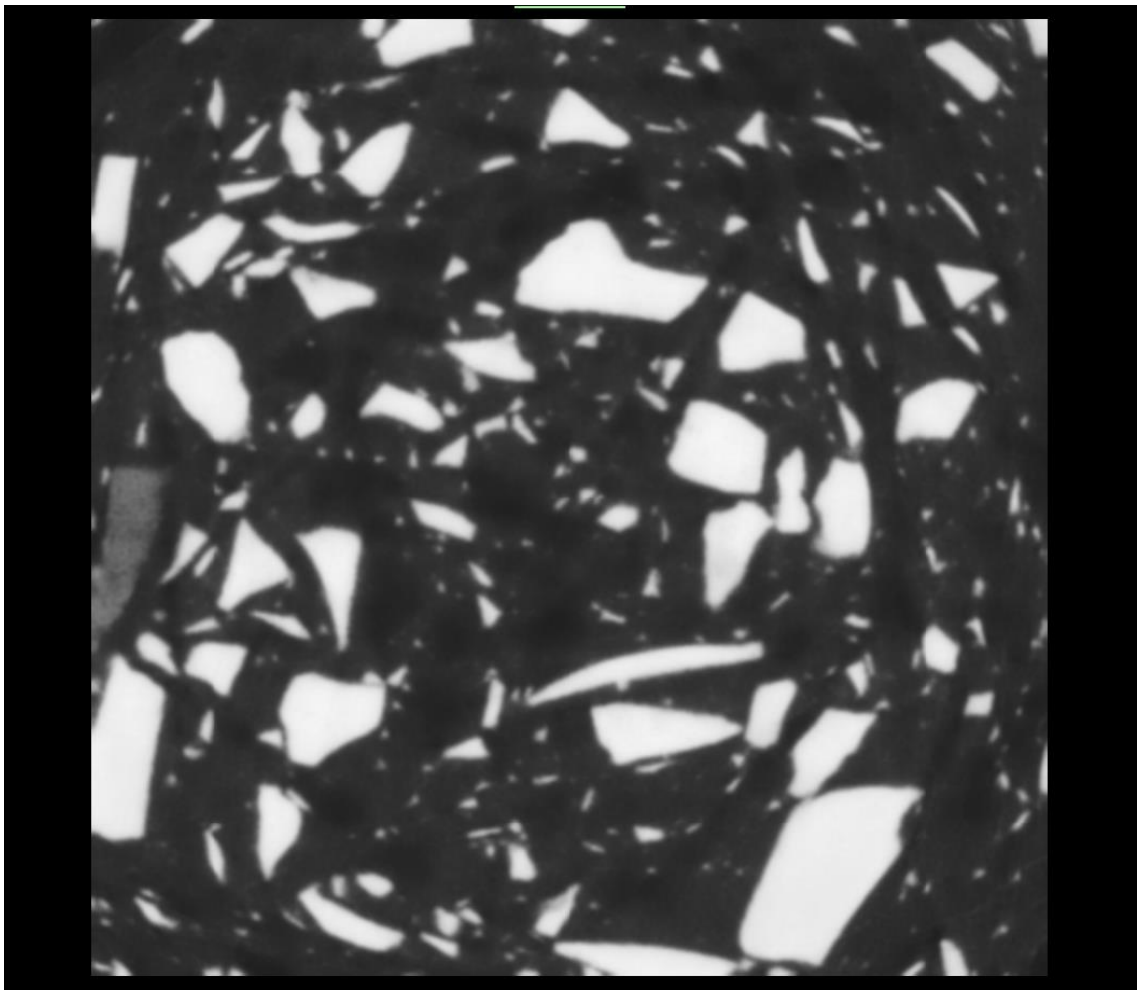

Figure 20. *400-projection reconstruction of particles and pores dataset enhanced with AI model number 23.*

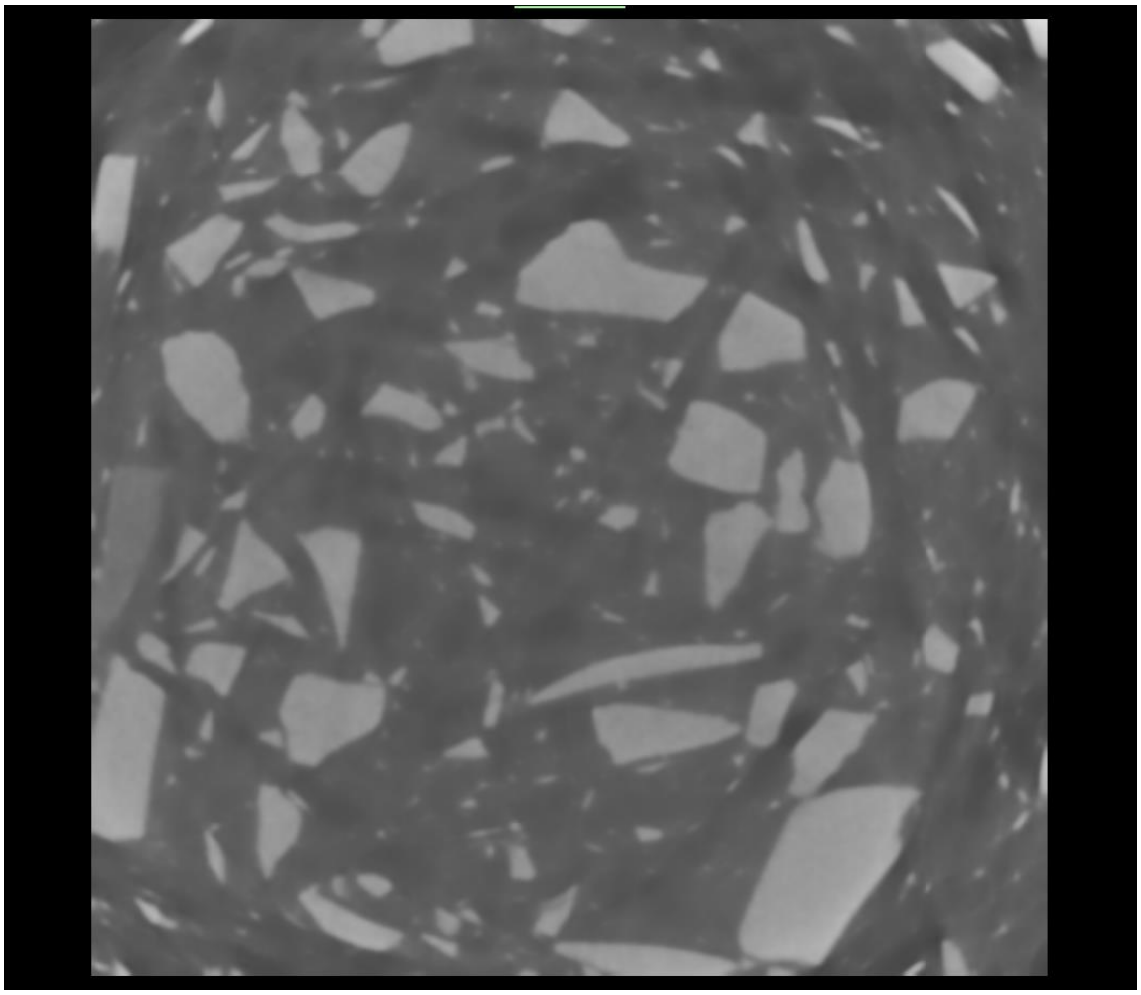

Figure 21. *800-projection reconstruction of particles and pores dataset enhanced with AI model number 22.*

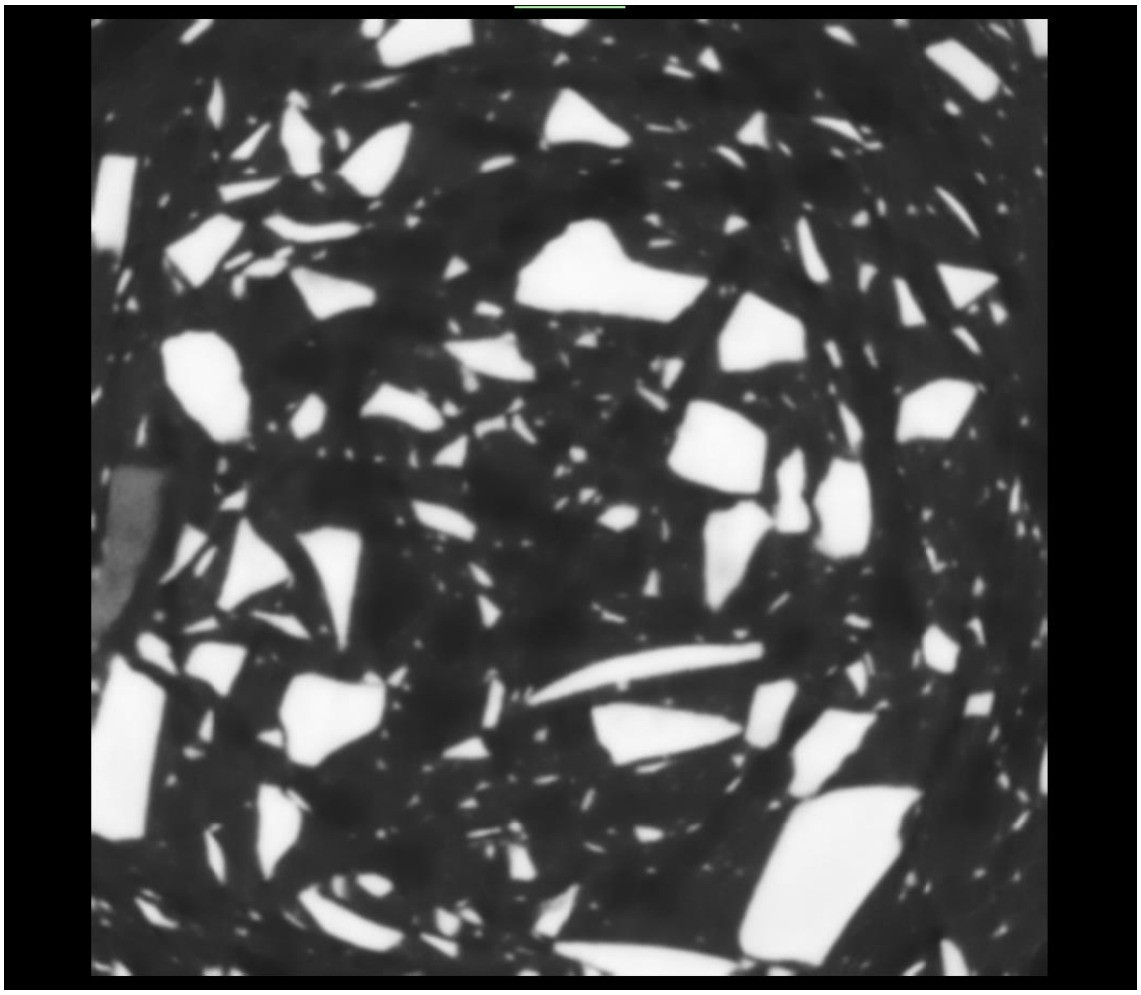

Figure 22. *800-projection reconstruction of particles and pores dataset enhanced with AI model number 22.*

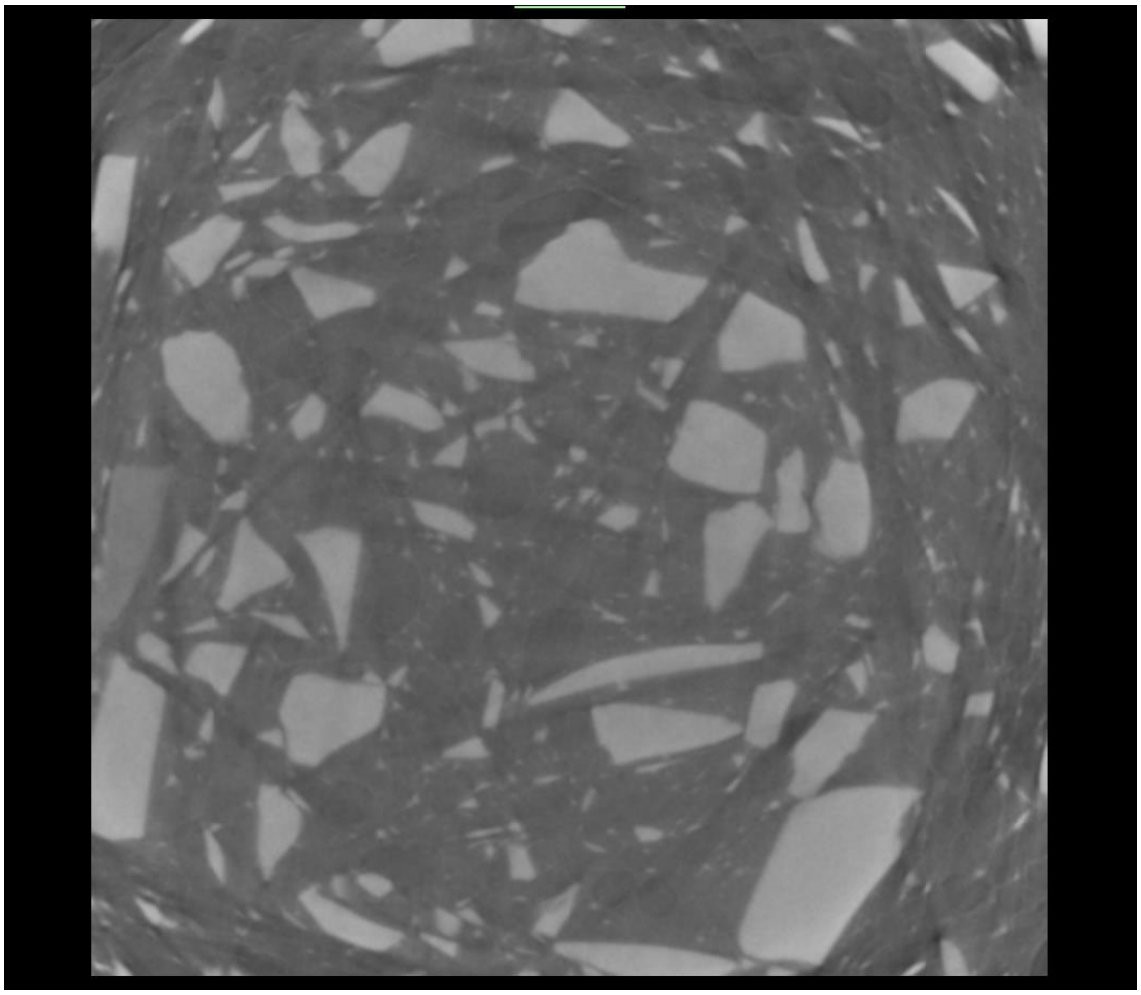

Figure 23. *1600-projection reconstruction of particles and pores dataset.*

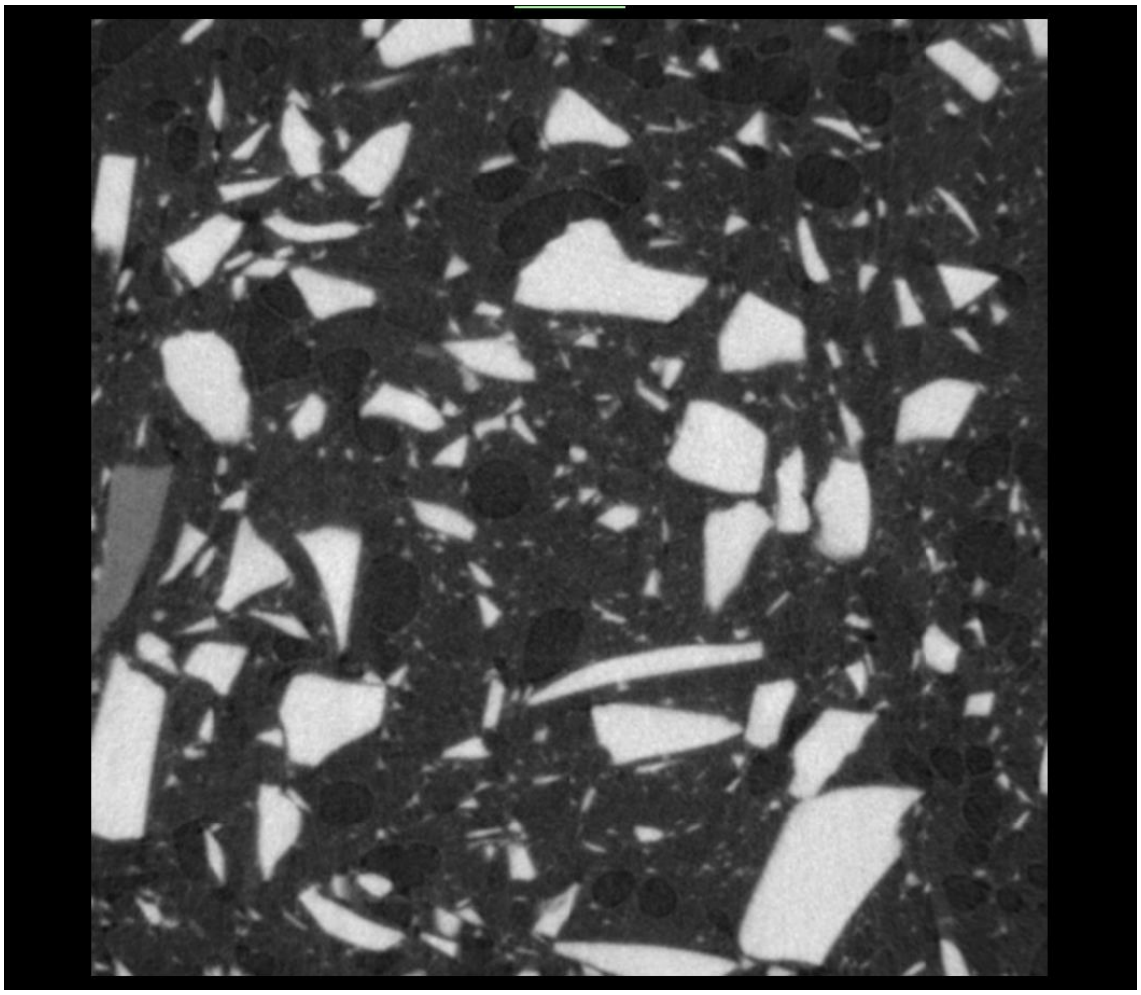

Figure 24. *1600-projection corrected reconstruction of particles and pores dataset.*

5.4 Training with different sample

The SNR calculations for the network training with different sample analysis are found in table 6. The SNR value of the original 1600-projection reconstruction was 15,62.

Table 6. The SNR calculations of the network training with different sample analysis. AI model number refers to the numbers presented in appendix B. The image name refers to the sample and the projection count of the reconstruction.

		SNR		
Training dataset	AI model number	Image		
		Pig eye 200	Pig eye 400	Pig eye 800
Original image		9,36	12,82	14,78
Particles	9	21,12	21,43	21,19
	15	15,28	20,43	21,00
	21	11,53	16,53	17,34
Pig eye	24	15,31	17,61	17,33
	25	13,39	16,37	16,53
	26	11,76	15,28	16,21

Figures 25 and 26 are example images of the 800-projection reconstruction. The images are enhanced with AI models number 9 and 24. Figure 27 is the 1600-projection reconstruction for comparison.

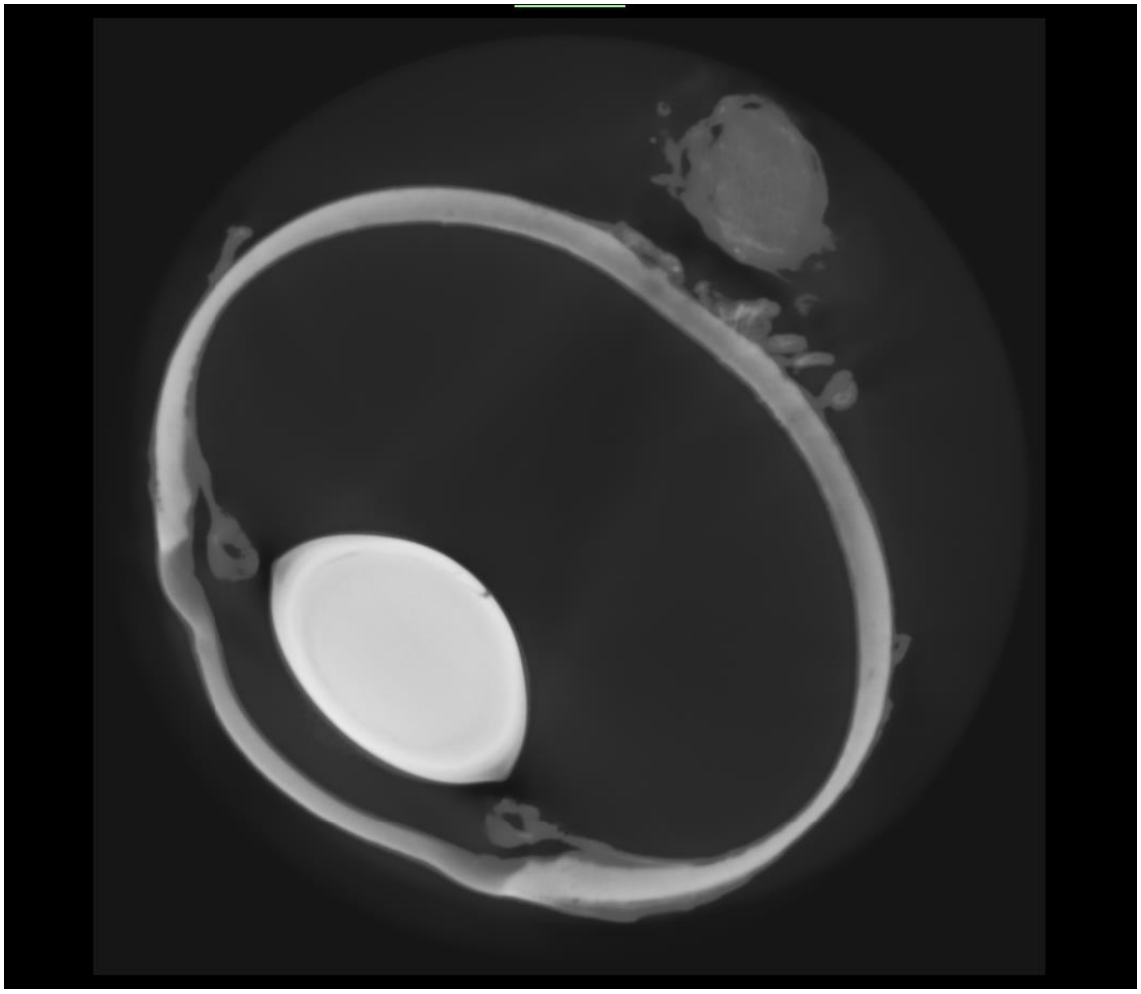

Figure 25. *800-projection reconstruction of the pig eye dataset enhanced with AI model number 9.*

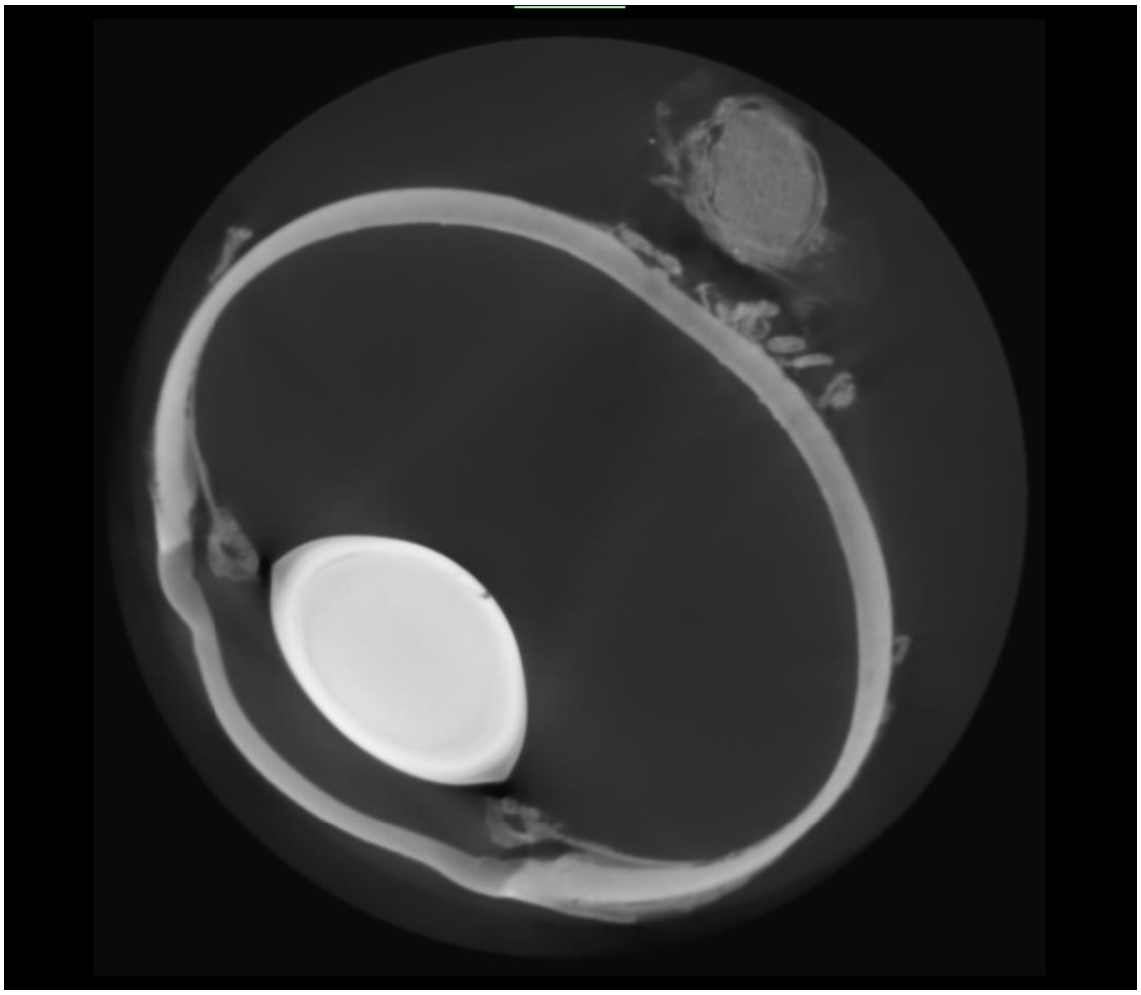

Figure 26. *800-projection reconstruction of the pig eye dataset enhanced with AI model number 24.*

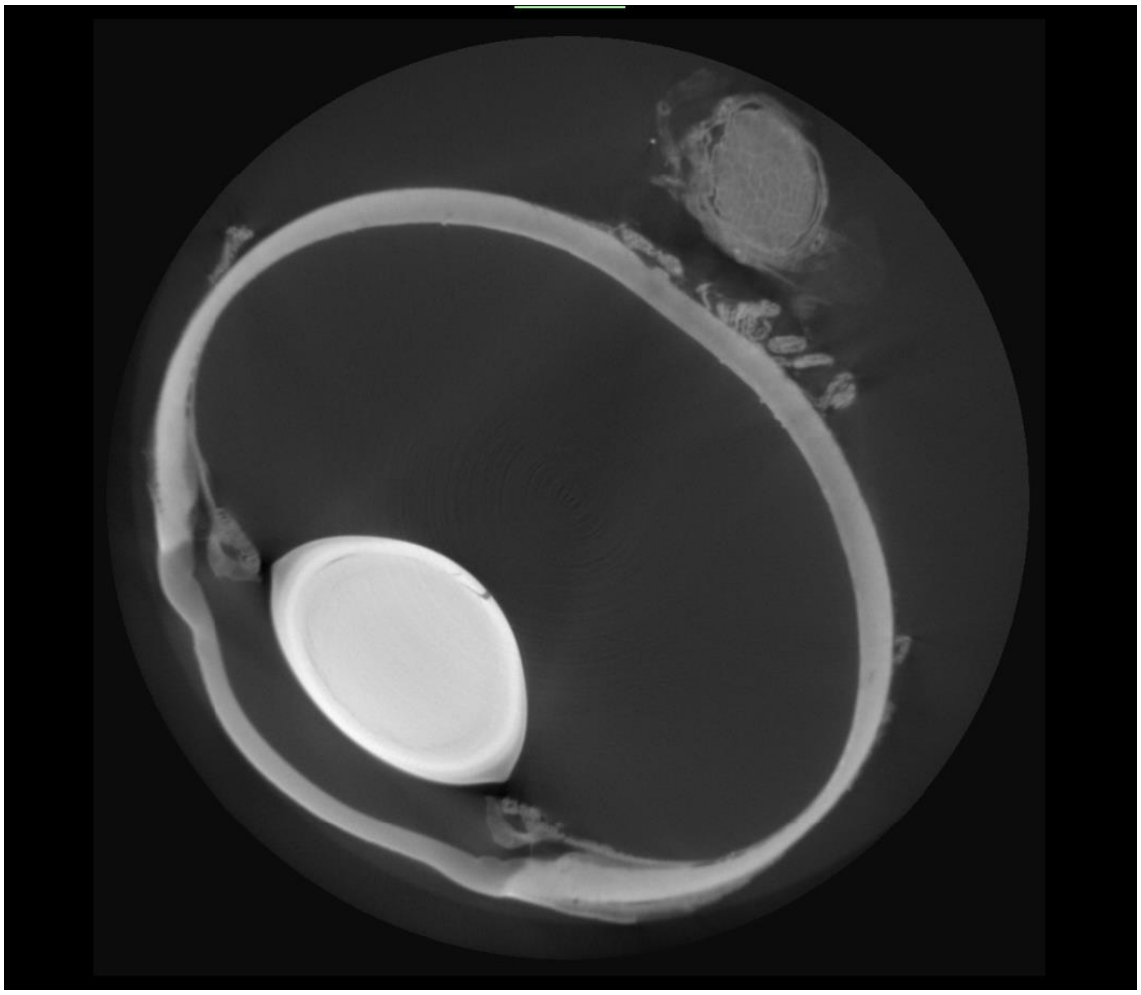

Figure 27. *1600-projection reconstruction of the pig eye dataset.*

5.5 Photon count and exposure time

The SNR calculations for the photon count and exposure time analysis are found on tables 7 and 8. Table 7 contains the results using the images obtained with absorption contrast imaging and table 8 contains the results using the images obtained with phase contrast imaging. The line intensity profiles of the different image enhancements are found in appendix F.

Table 7. The SNR calculations of the network training with different photon count (absorption contrast imaging) analysis. AI model number refers to the numbers presented in appendix B. The image name refers to the sample and the photon count of the reconstruction.

SNR						
Training output data (number of photons)	AI model number	Image				
		Pores and fibers 1800	Pores and fibers 3500	Pores and fibers 7000	Pores and fibers 14000	Pores and fibers 5000
Original image		4,45	4,53	4,61	4,68	3,58
5000	27	3,05	3,18	-	-	-
7000	28	5,10	5,06	-	-	-
14000	29	4,94	4,99	-	-	-

Table 8. The SNR calculations of the network training with different photon count (phase contrast imaging) analysis. AI model number refers to the numbers presented in appendix B. The image name refers to the sample and the photon count of the reconstruction.

SNR				
Training input data (number of photons)	AI model number	Image		
		Pores and fibers 400	Pores and fibers 3000	Pores and fibers 6000
Original image		4,05	4,76	4,84
400	30	5,68	6,03	-
3000	31	4,74	5,07	-

Figures 19, 20 and 21 are example images of the 1800 photon reconstruction. The images are enhanced with AI models number 27, 28 and 29. Figures 22 and 23 are example images of the 400 photon reconstruction. The images are enhanced with AI models number 30 and 31.

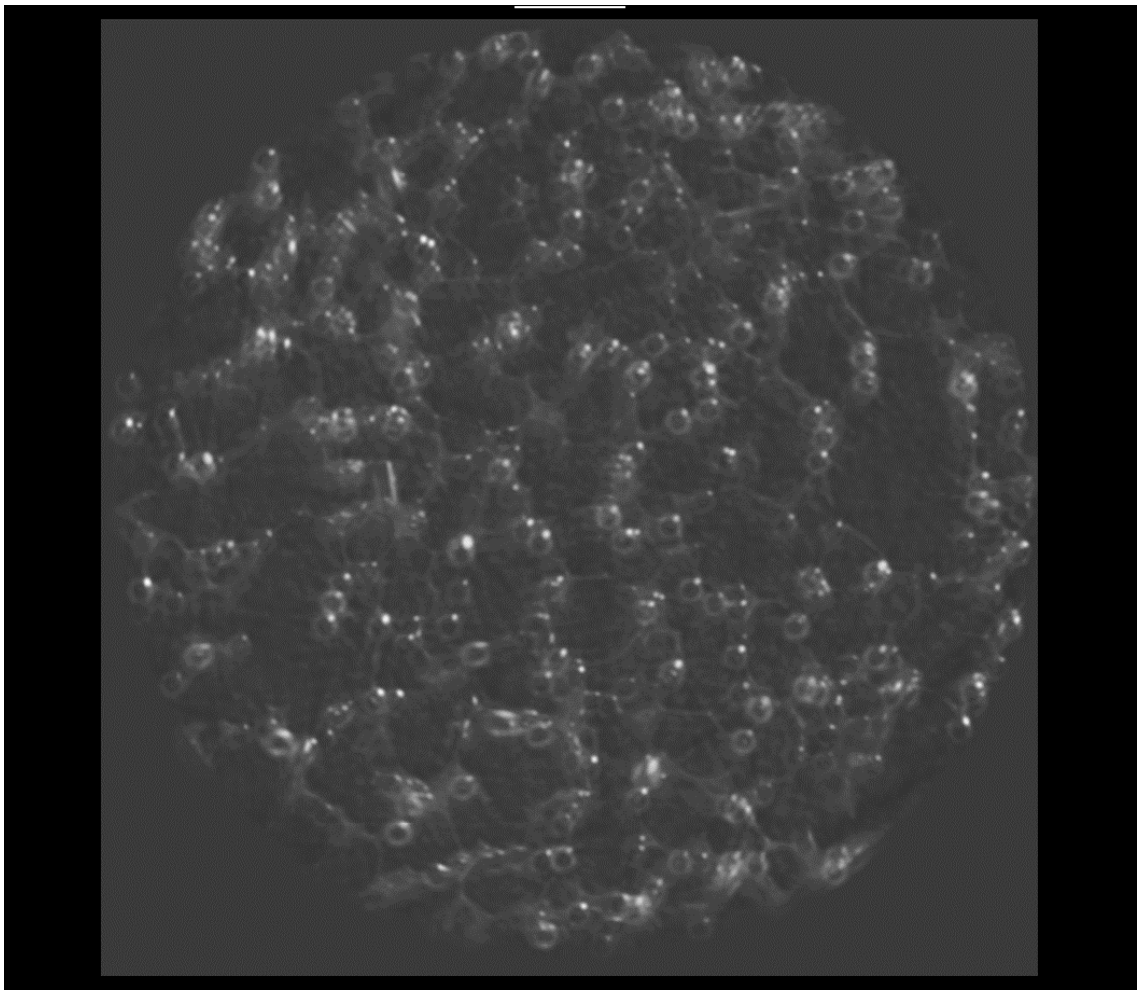

Figure 28. *1800 photon reconstruction of the pores and fibers (absorption contrast) dataset enhanced with AI model number 27.*

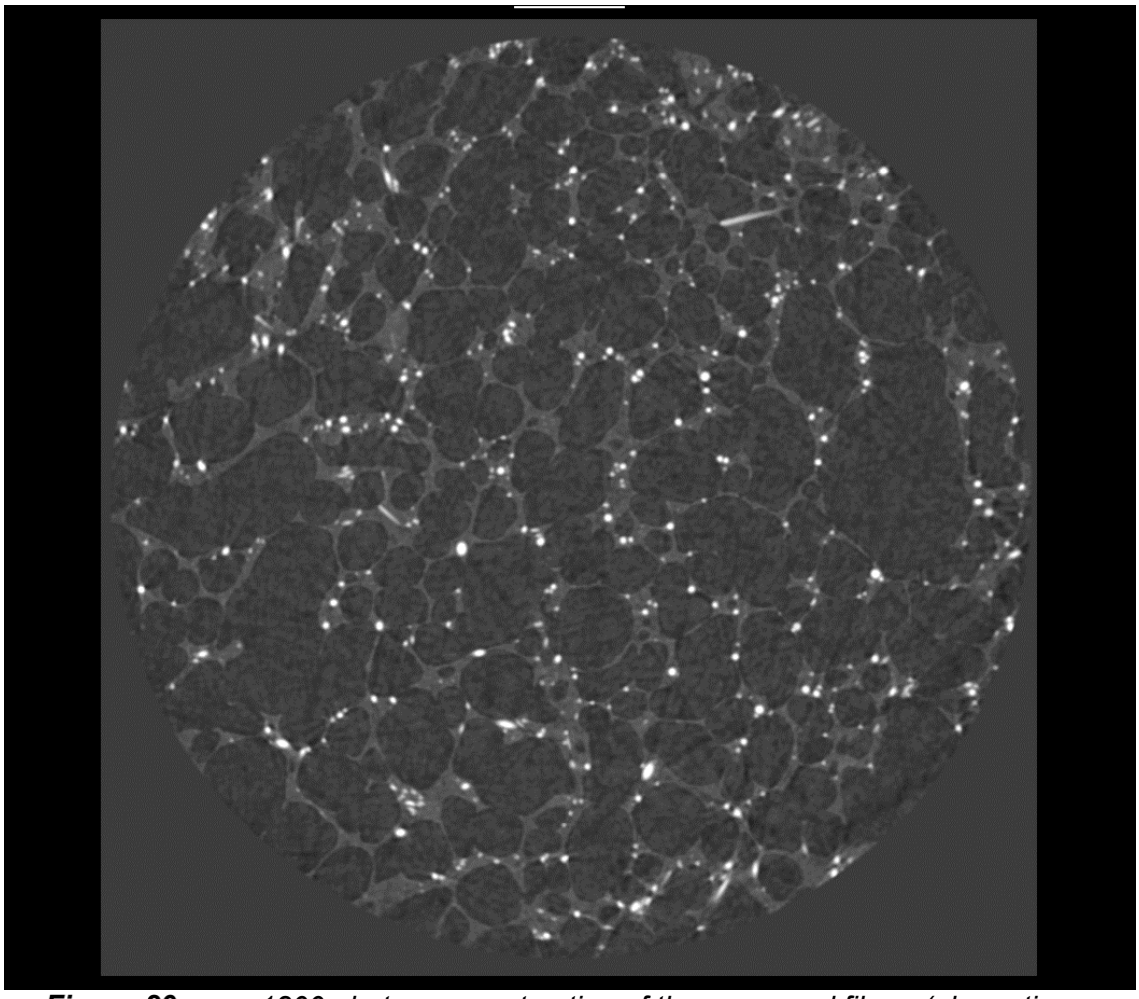

Figure 29. *1800 photon reconstruction of the pores and fibers (absorption contrast) dataset enhanced with AI model number 28.*

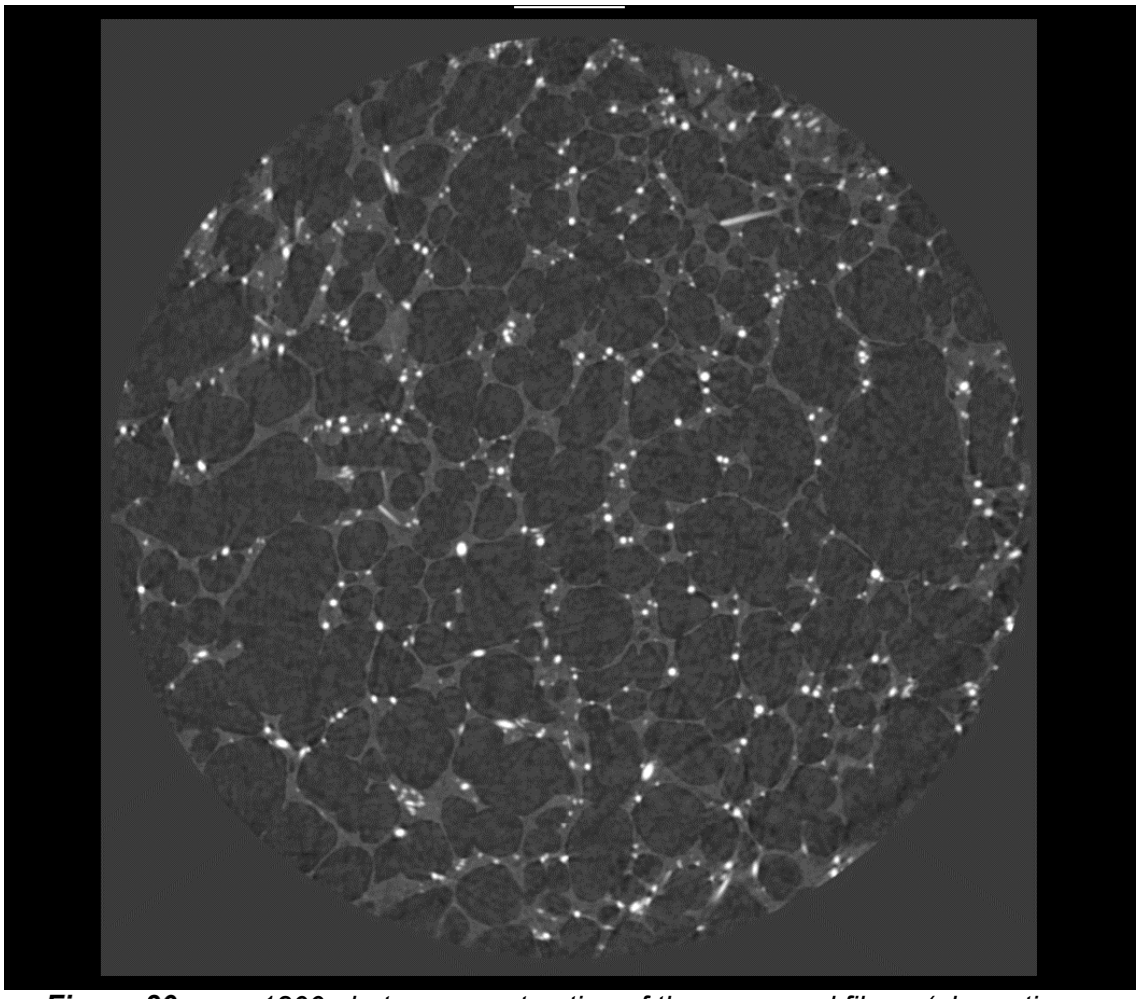

Figure 30. *1800 photon reconstruction of the pores and fibers (absorption contrast) dataset enhanced with AI model number 29.*

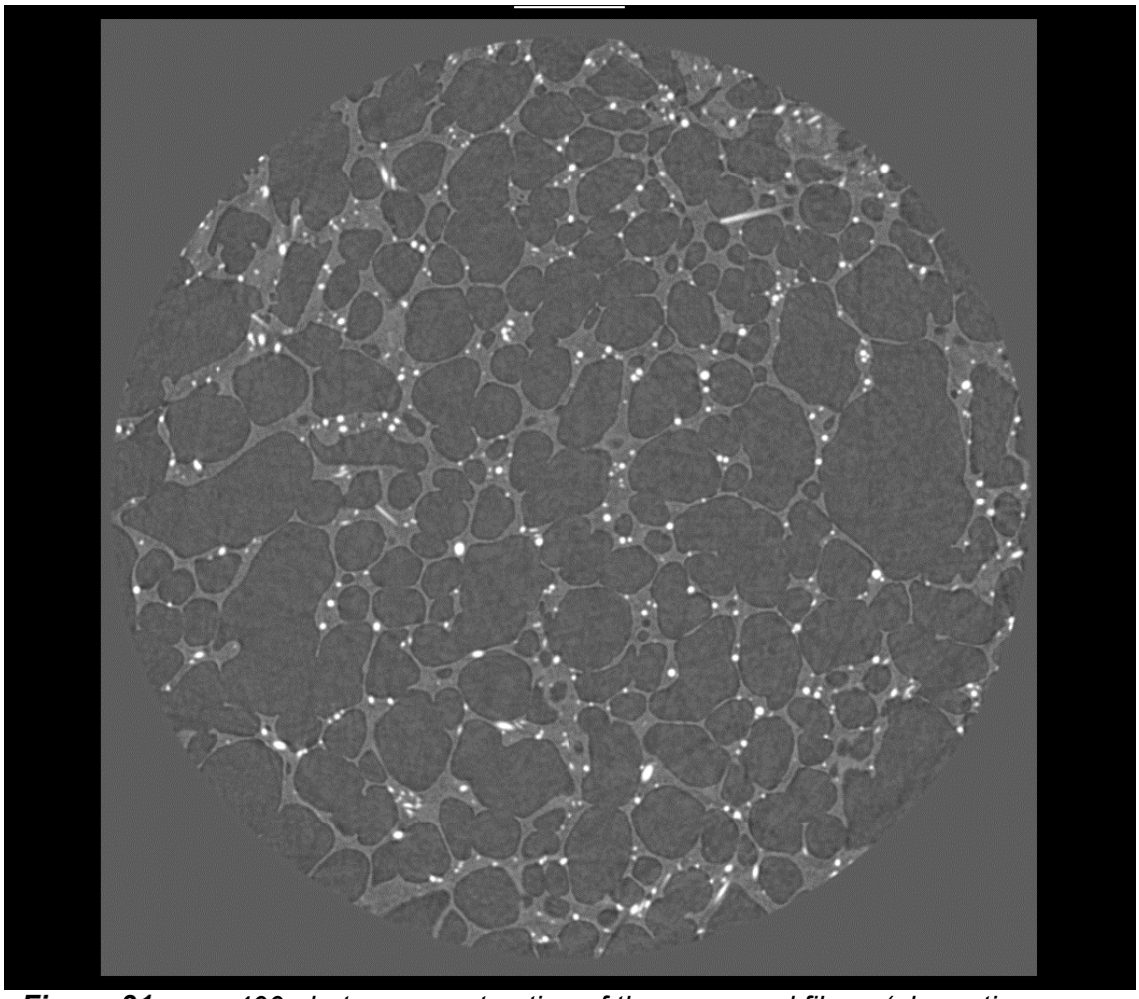

Figure 31. *400 photon reconstruction of the pores and fibers (absorption contrast) dataset enhanced with AI model number 30.*

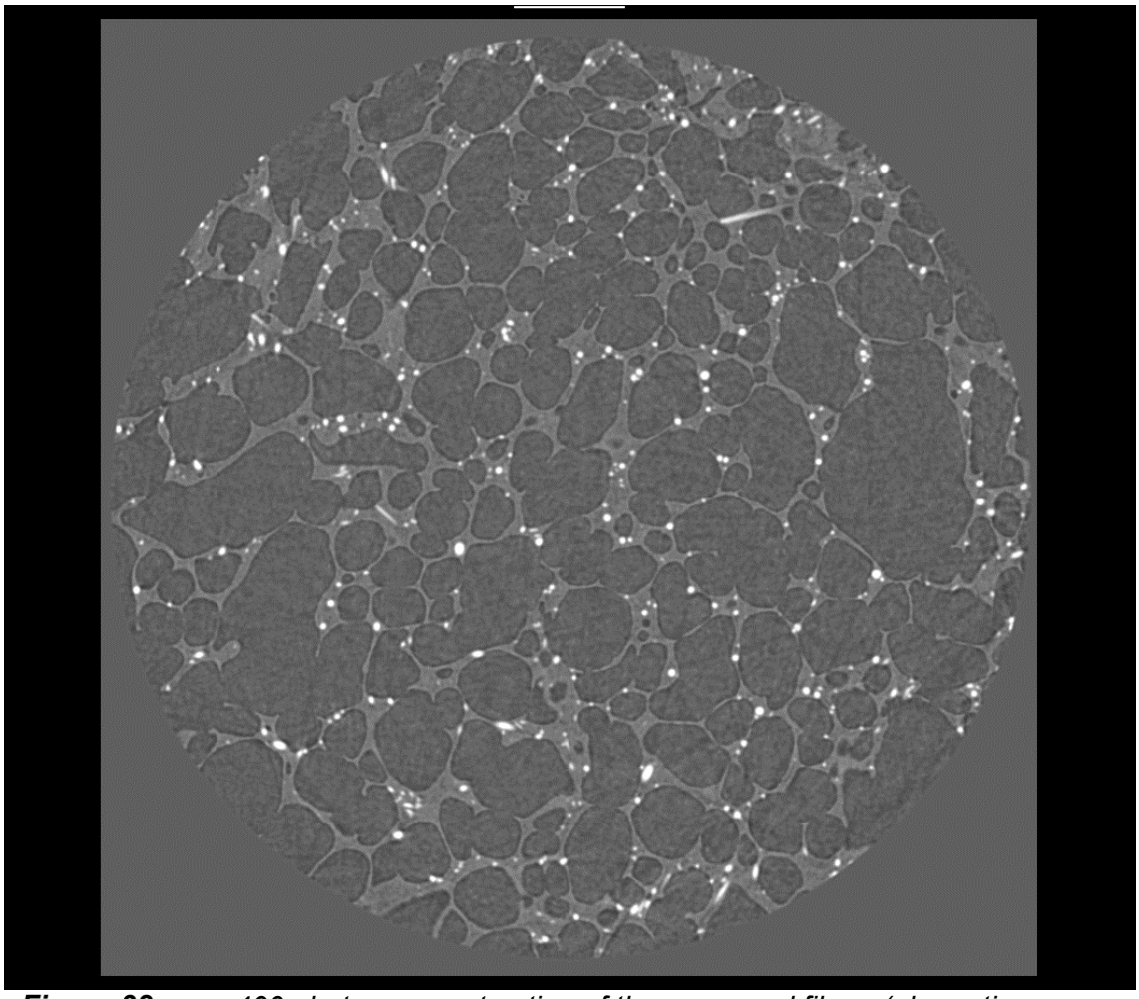

Figure 32. *400 photon reconstruction of the pores and fibers (absorption contrast) dataset enhanced with AI model number*

6. DISCUSSION

In this master's thesis the abilities of artificial intelligence to enhance μ-CT images were tested. There were four different samples that were imaged. The images from the samples were reconstructed with different number of projections to be able to study if images with lower projection count and worse quality can be enhanced enough to make them a feasible option for imaging. With lower projection count the imaging time and consequently the radiation dose could be lowered for imaging subjects.

First the best network architecture was needed to find out from the Dragonfly software. From the SNR calculations in table 2 can be seen that there are little differences in the SNR values. The line intensity profiles in appendix D, and figures 42 and 43 show that U-Net has slightly better abilities to reduce noise and maintain the best similarity in internal structures. For these reason U-Net was chosen as the network architecture for the rest of the network trainings.

In the second part when examining the effects of input data quality there were networks trained with varying input image projection counts and input slice counts. The results seen in table 3 tell that the quality of the 100-projection reconstruction is too poor to be enhanced or have any use, when compared to the SNR-value of the 1600-projection reconstruction from 5.1. Due to these results the 100-projection reconstruction will not be used in the later parts. In table 4 there are also relative SNR changes from table 3. From these tables can be seen that the networks trained with 200-projection reconstruction have greatly improved SNR values. The SNR values are quite similar for all of the different images at around 10 to 15. But the low quality of the input data will modify some of the internal structures as seen in the line intensity profiles of the architecture examination in appendix D.

The networks trained with 400-projection reconstruction have much more different effects on the images enhanced. The 200-projection images quality stays roughly the same. 400-projection images are the best quality when enhanced with these networks. The quality of the 800-projections images is also a little better. As for the 800-projection networks, they are able to enhance only the 400 and 800 projection images and not even very much. This might be due to the lower noise level in the input image which correlates to the networks ability to denoise. The input slice count has little to none effect on the SNR values. In most cases there is slight increase in SNR with higher slice counts but nothing that would be considerable enough.

The examination of the quality of the output gave very straight forward results in table 5. The SNR value stays pretty much the same when enhancing the images with network trained with the original output image. But when enhancing with the network trained with the corrected output data the SNR values rise from 4 to 15. The line intensity profiles in appendix E also show that the boundaries of internal structures are sharper with the corrected output image enhancements.

In the fourth test there were networks with different training data. In table 6 can be seen the results that show that the images enhanced with networks trained with projection data have higher SNR values than the ones enhanced with networks trained with pig eye data. This is due to the lack of structures in the particles data. It is able to denoise the image more but also “flattens” it by compressing the intensity values closer to its own. As the pig eye images have more complex structures there will be some data loss.

The final test shows that there are not enough differences between the enhanced images with different exposure times. In tables 7 and 8 are the SNR values for the images and the values are not improved very much. This is also noticed when examining figures 29, 30, 31, and 32. Also the line intensity profiled in appendix F show that there are practically no improvements in the image quality that can be observed. The 5000 photon image had a little offset compared to the other images which explains figure 28 and the SNR values in table 7. To gain more competent results about the effects of photon count and exposure time on image quality there should be more extensive research with more image data.

With the results combined the best enhancing capabilities would be gained creating a U-Net network trained with similar dataset as the enhanced images are to make sure there will not be too much data loss. The output data should also be filtered or segmented in advance for better enhancing properties. 100 and 200 projection reconstruction are not likely to have use as the image quality suffers too much. 400 and 800 projection reconstructions gave the best results in order of acquiring better quality and not losing too much data. These reconstructions might have some clinical use in some cases with the right AI networks. With lower projection counts less radiation and shorter imaging times are a possibility. These results are best applied with Dragonfly software but are feasible to implement with other AIs.

As the input slice count had little effect, more of its effects could be examined with other AIs that could have larger slice count than 11 which was the upper limit on the software used in this thesis. Other AIs also have different network models which could make some different results. As only three networks were examined, it is not likely to find the optimal

network. For future research it would also be possible to examine if it is possible to enhance the projection data before the reconstruction or train one network with multiple different datasets. Also some artificial noise could be added to the training data to see if it would improve the denoising capabilities without lowering overall quality. All in all, AI clearly has its use in enhancing μ-CT images with a lot of training data and proper implementations of AI.

REFERENCES

[1] McCollough,, C. H., & Leng, S. (2020). Use of artificial intelligence in computed tomography dose optimization. Ann ICRP. Dec;49(1_suppl): 113-125.

[2] Li, H., Zhang, H., Tang, Z. & Hu G. (2008). Micro-computed tomography for small animal imaging: Technological details. Progress in Natural Science. 18(5), pp. 513-521.

[3] Bushberg, J. (2002). The Essential Physics of Medical Imaging. Philadelphia: Lippincott Williams & Wilkins.

[4] Carroll, Q. (2011). Radiography in the Digital Age: Physics, Exposure, Radiation Biology. Springfield, Ill.: Charles C. Thomas.

[5] Beutel, J., Kundel, H. and Van Metter R. (2000). Handbook of medical imaging. Bellingham, Washington, USA: SPIE Press.

[6] Mizutani, R. & Suzuki, Y. (2012). X-ray microtomography in biology. Micron. 43(2-3), pp. 104-115.

[7] Arhatari, B., De Carlo, F. & Peele, A. (2007) Direct quantitative tomographic reconstruction for weakly absorbing homogeneous phase objects. Review of Scientific Instruments. 78(5), pp. 053701 1-5.

[8] Rodriguez-Molares, A., Rindal, O.M.H., D'hoog, J., Masoy, S.-E., Austeng, A., Lediju Bell, M.A. & Torp, H. (2020). The Generalized Contrast-to-Noise Ratio: A Formal Definition for Lesion Detectability. IEEE Transactions on Ultrasonics, Ferroelectrics, and Frequency Control, 67(4), pp.745–759.

[9] Marsland, S. (2015). Machine Learning: An Algorithmic Perspective, second edition. CRC Press.

[10] Alpaydin, E. (2010). Introduction to Machine Learning [Sl].

[11] Mohri, M., Rostamizadeh, A. & Talwalkar, A. (2012). Foundations of machine learning. MIT press.

[12] Ting, D.S.W., et al. (2018). AI for medical imaging goes deep. Nat Med 24, 539–540.

[13] Xing, L., Giger, M. L., & Min, J. K. (2021). Artificial intelligence in medicine: Technical basis and clinical applications. London, United Kingdom: Academic Press

[14] LeCun, Y., Bottou, L., Bengio, Y., & Haffner, P. (1998). Gradient-based learning applied to document recognition. Proceedings of the IEEE, 86(11), 2278-2324.

[15] Heaton, J. (2015). Artificial Intelligence for Humans, Volume 3: Deep Learning and Neural Networks. Heaton Research Inc, USA.

[16] Machine Learning (https://www.britannica.com/technology/machine-learning)

[17] Lipto, Z., Berkowitz J., Elkan, C. (2015). A Critical Review of Recurrent Neural Networks for Sequence Learning. arXiv preprint arXiv:1506.00019.

[18] Canedo, D. & Romariz, A. (2018). Data Analysis of Wireless Networks Using Computational Intelligence. Journal of Communications. 13. 618-626. 10.12720/jcm.13.11.618-626.

[19] Cortes, C., Vapnik, V. (1995). Support-Vector Networks. Machine Learning 20, 273-297

[20] Boehmke, B., & Greenwell, B. (2019). Hands-On Machine Learning with R (1st ed.). Chapman and Hall/CRC.

[21] Patterson, J., & Gibson, A. (2017). Deep Learning; A Practioner's Approach.

[22] Socher, R., Lin, C. C., Manning, C., & Ng A. Y. (2011). Parsing natural scenes and natural language with recursive neural networks. In Proceedings of the 28th international conference on machine learning (ICML-11) (pp. 129-136).

[23] Graves, A. (2012). Supervised sequence labelling. In Supervised sequence labelling with recurrent neural networks (pp. 5-13). Springer, Berlin, Heidelberg.

[24] Vincent, P., Larochelle H., Lajoie I., Bengio Y., & Manzagol P. A. (2010). Stacked denoising autoencoders: Learning useful representations in a deep network with a local denoising criterion. Journal of machine learning research, 11(Dec), 3371-3408.

APPENDIX A: REFERENCE IMAGES OF THE SAMPLES

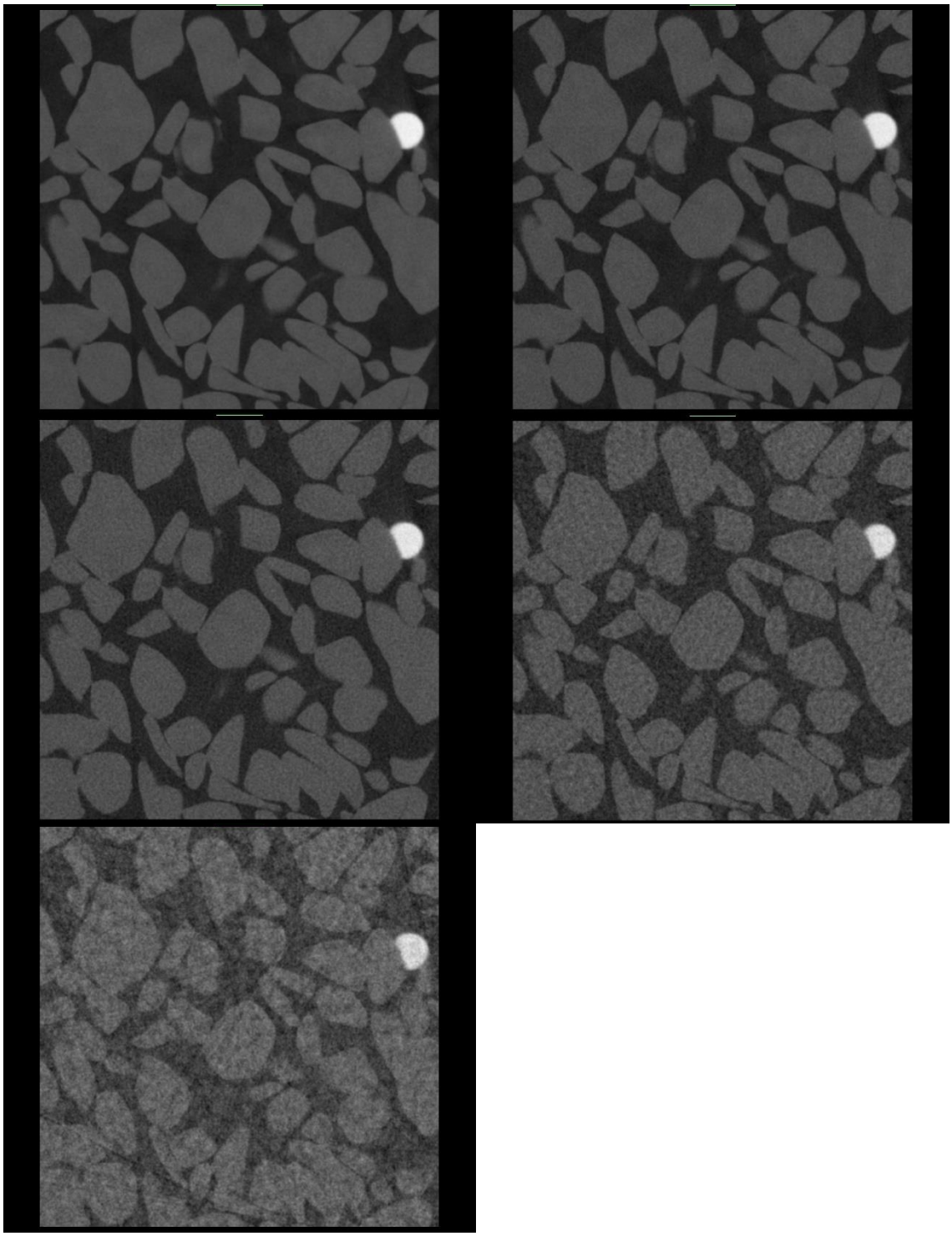

Figure 33. *Particles dataset. From upper-left corner 1600, 800, 400, 200, and 100 projection reconstructions.*

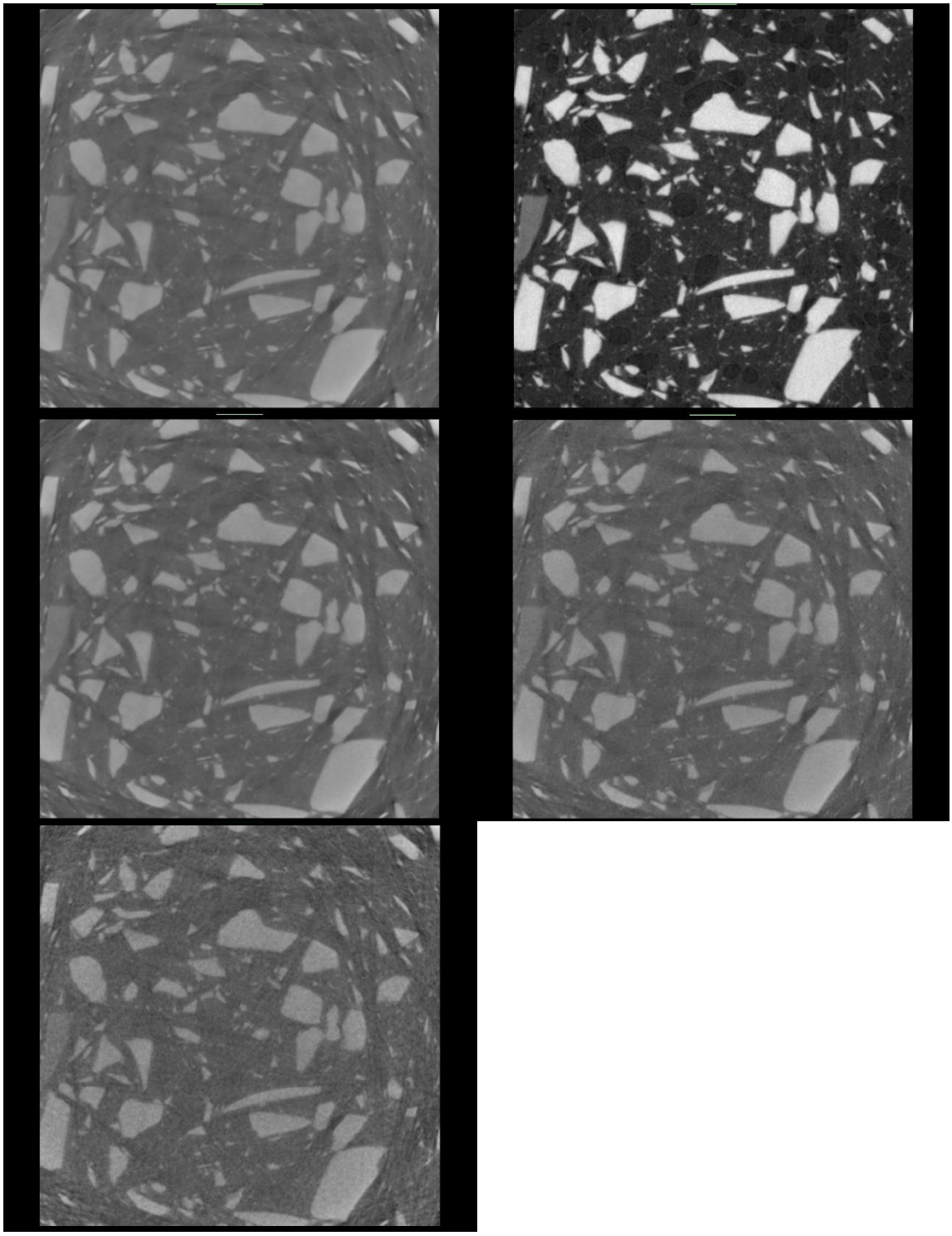

Figure 34. *Particles and pores dataset. From upper-left corner 1600, 1600(corrected), 800, 400, and 200 projection reconstructions.*

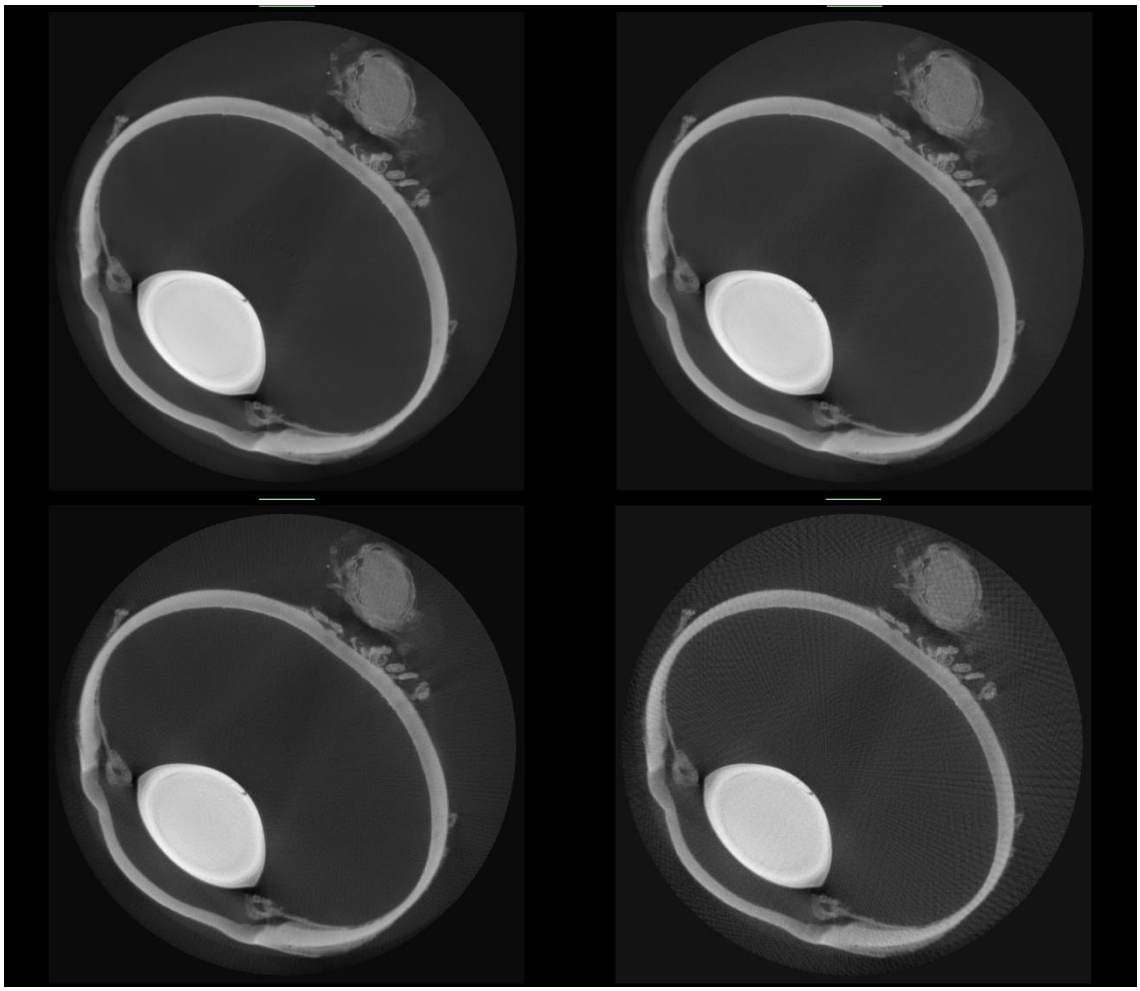

Figure 35. *Pig eye dataset. From upper-left corner 1600, 800, 400, and 200 projection reconstructions.*

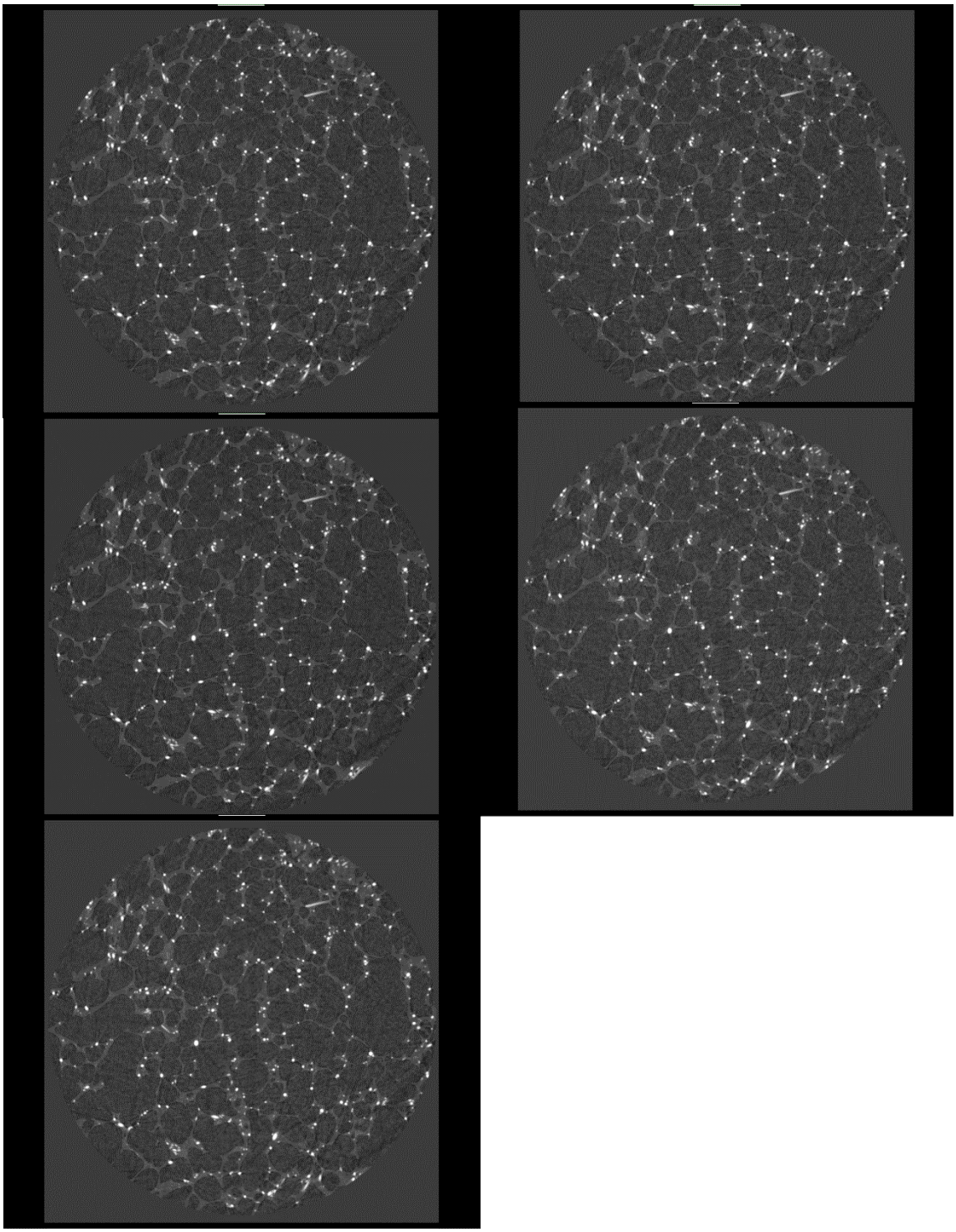

Figure 36. *Pores and fibers (absorption contrast) dataset. From upper-left corner 14000, 7000, 5000, 3500 and 1800 photon reconstructions.*

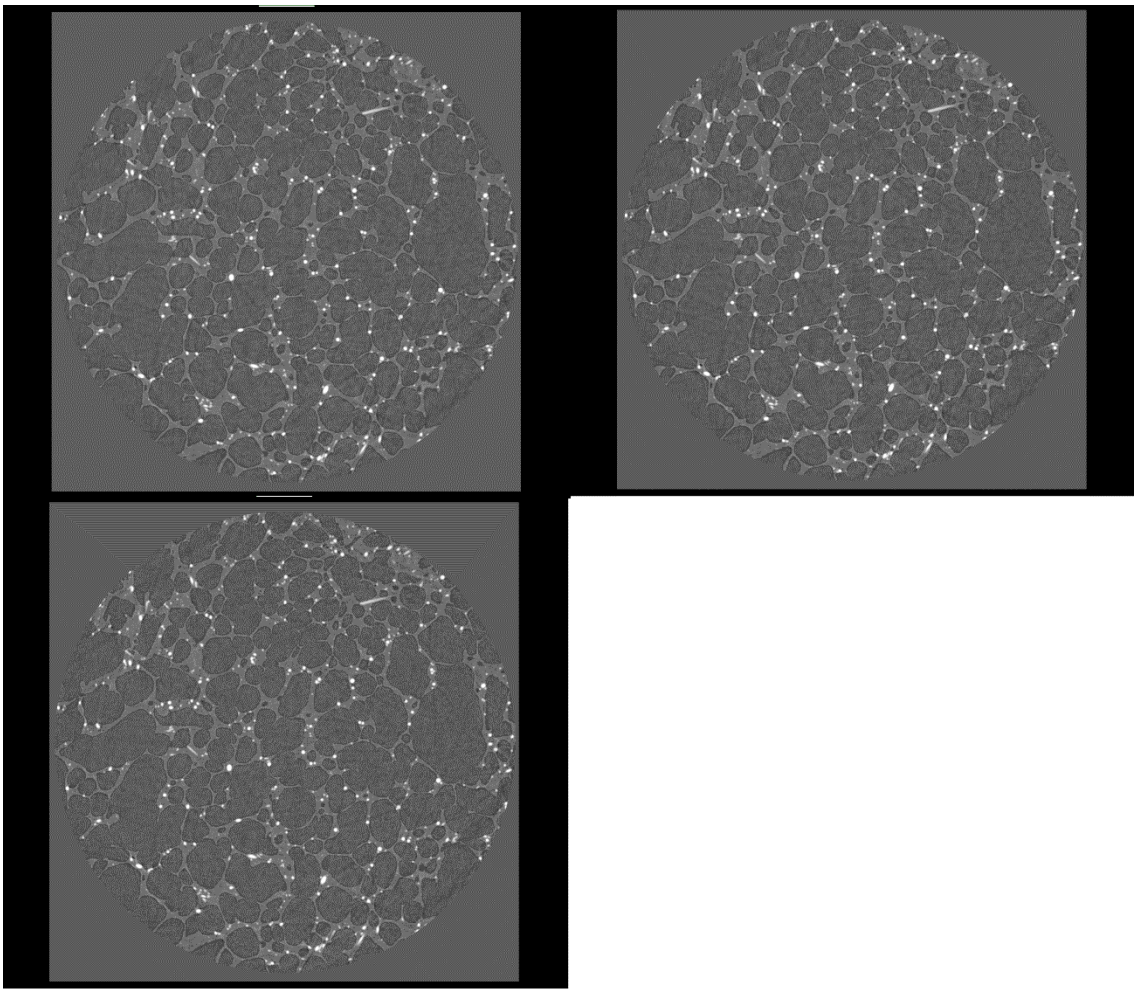

Figure 37. *Pores and fibers (phase contrast) dataset. From upper-left corner 6000, 3000 and 400 photon reconstructions.*

APPENDIX B: AI MODELS

Table 9. List of AI models trained for the thesis.

Image sample	Model architechture	Input slice count	Input projection count (+photon count for pores and fibers)	Output projection count (+photon count for pores and fibers)	Number of model
Particles	Auto-Encoder	1	200	1600	1
	Noise2Noise	1	200	1600	2
	U-Net	1	100	1600	3
		1	200	1600	4
		3	200	1600	5
		5	200	1600	6
		7	200	1600	7
		9	200	1600	8
		11	200	1600	9
		1	400	1600	10
		3	400	1600	11
		5	400	1600	12
		7	400	1600	13
		9	400	1600	14
		11	400	1600	15
		1	800	1600	16
		3	800	1600	17
		5	800	1600	18
		7	800	1600	19
		9	800	1600	20
		11	800	1600	21
Particles and pores	U-Net	1	200	1600	22
		1	200	1600 (corrected version)	23
Pig eye	U-Net	11	200	1600	24
		11	400	1600	25
		11	800	1600	26
Pores and fibers (absorption)	U-Net	11	1600/1800	3200/5000	27
		11	1600/1800	1600/7000	28
		11	1600/1800	1600/14000	29
Pores and fibers (phase contrast)	U-Net	11	1600/400	1600/6000	30
		11	1600/3000	1600/6000	31

APPENDIX C: STANDARD DEVIATION AREAS AND LINE PLACEMENTS

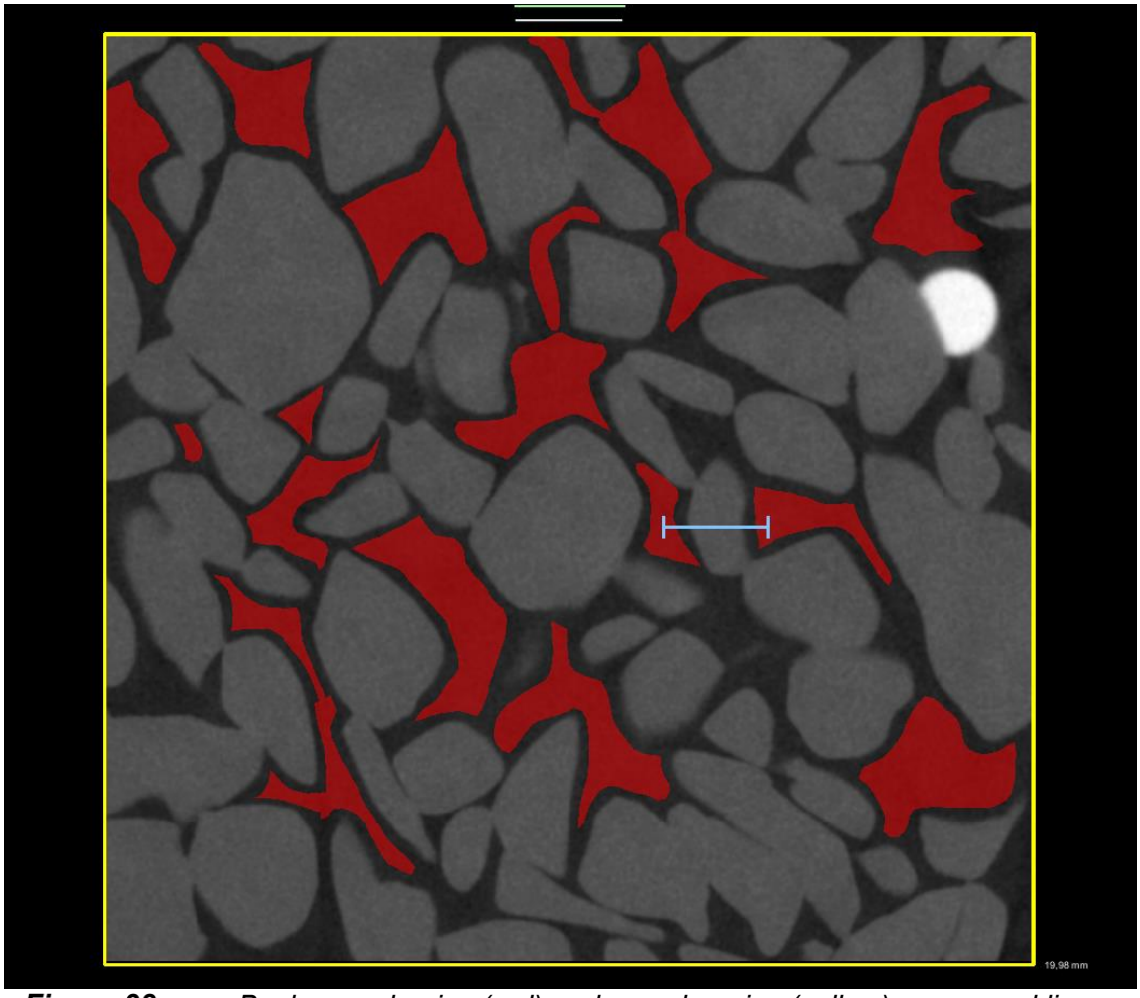

Figure 38. *Background noise (red) and sample noise (yellow) areas, and line intensity placement (blue) in particles dataset.*

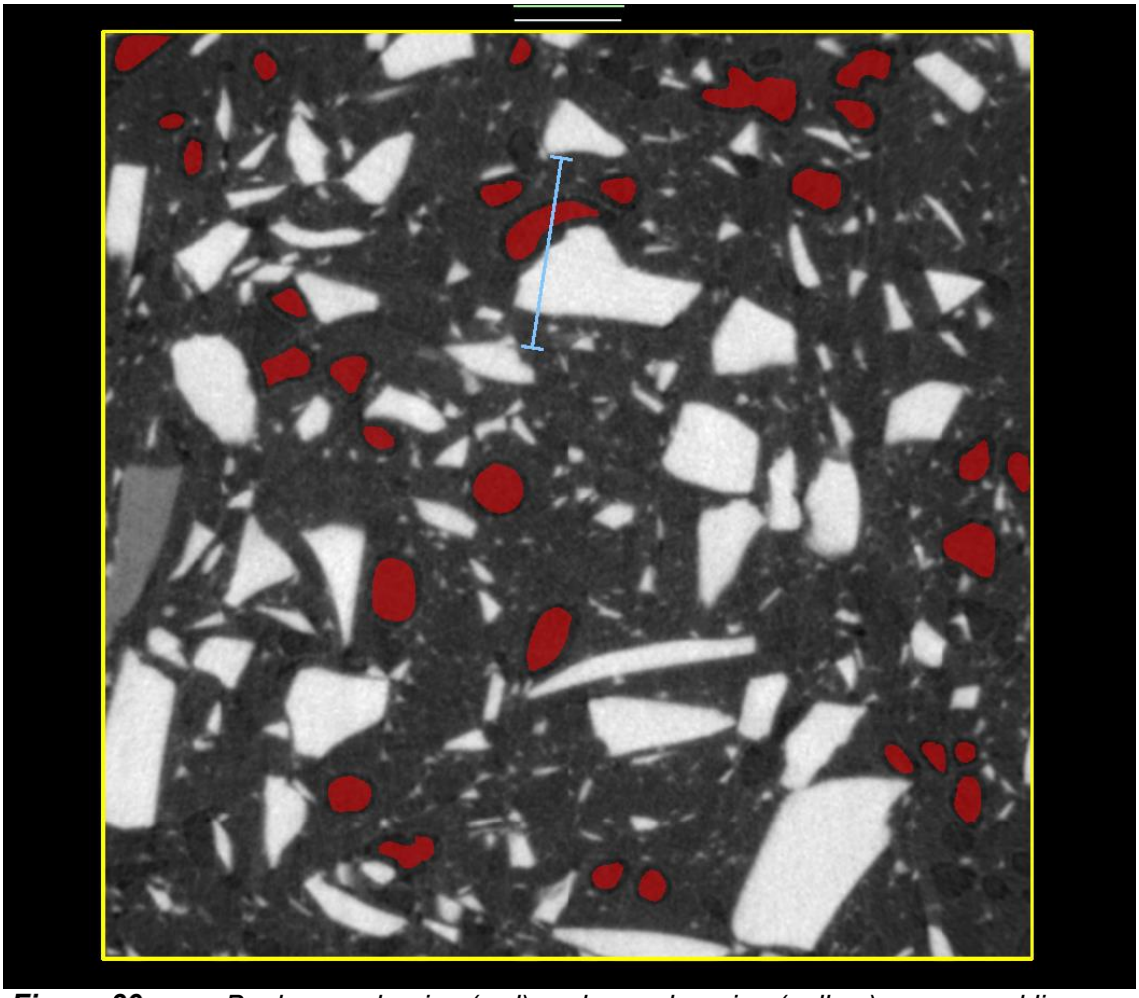

Figure 39. *Background noise (red) and sample noise (yellow) areas, and line intensity placement (blue) in particles and pores dataset.*

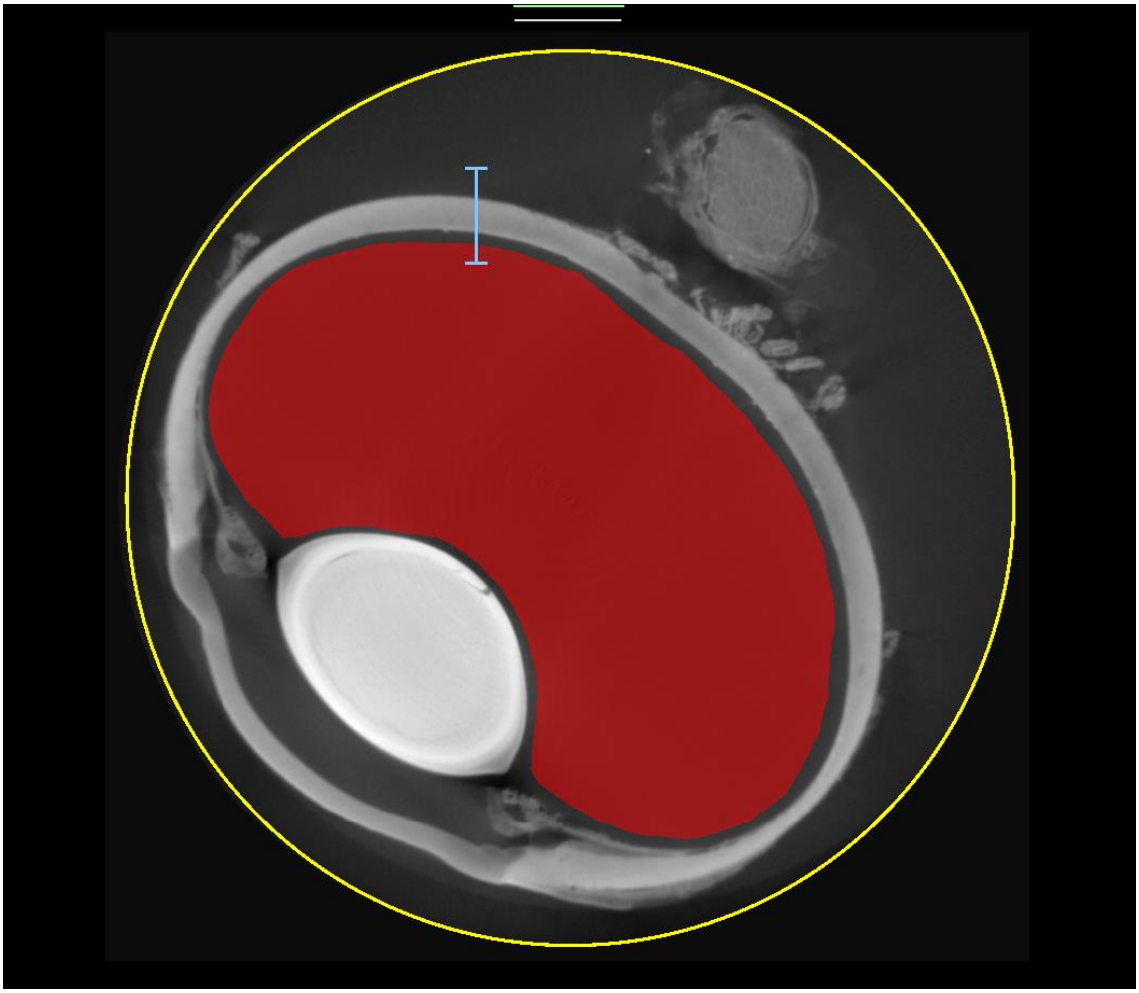

Figure 40. *Background noise (red) and sample noise (yellow) areas, and line intensity placement (blue) in pig eye dataset.*

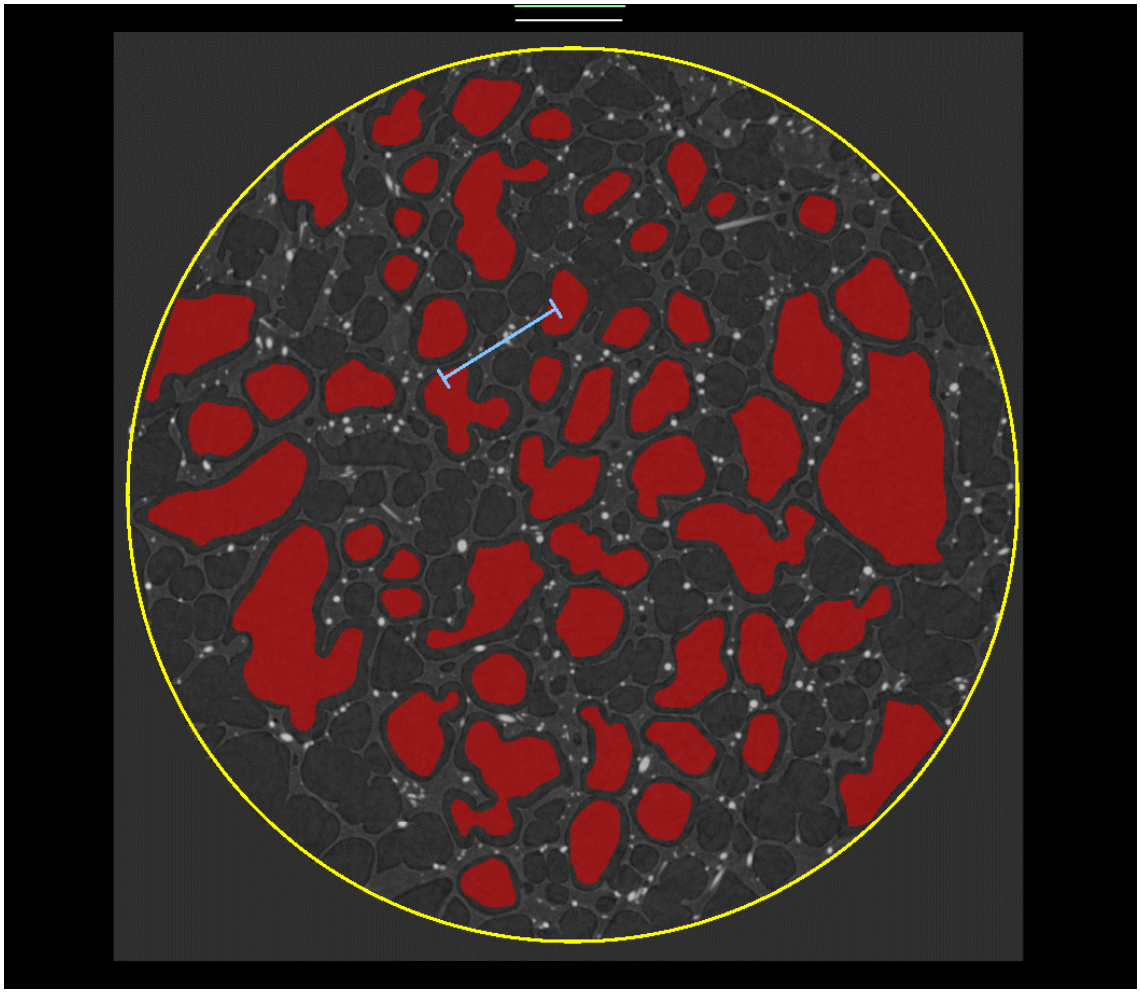

Figure 41. *Background noise (red) and sample noise (yellow) areas, and line intensity placement (blue) in pores and fibers dataset.*

APPENDIX D: ARCHITECTURE LINE INTESITIES

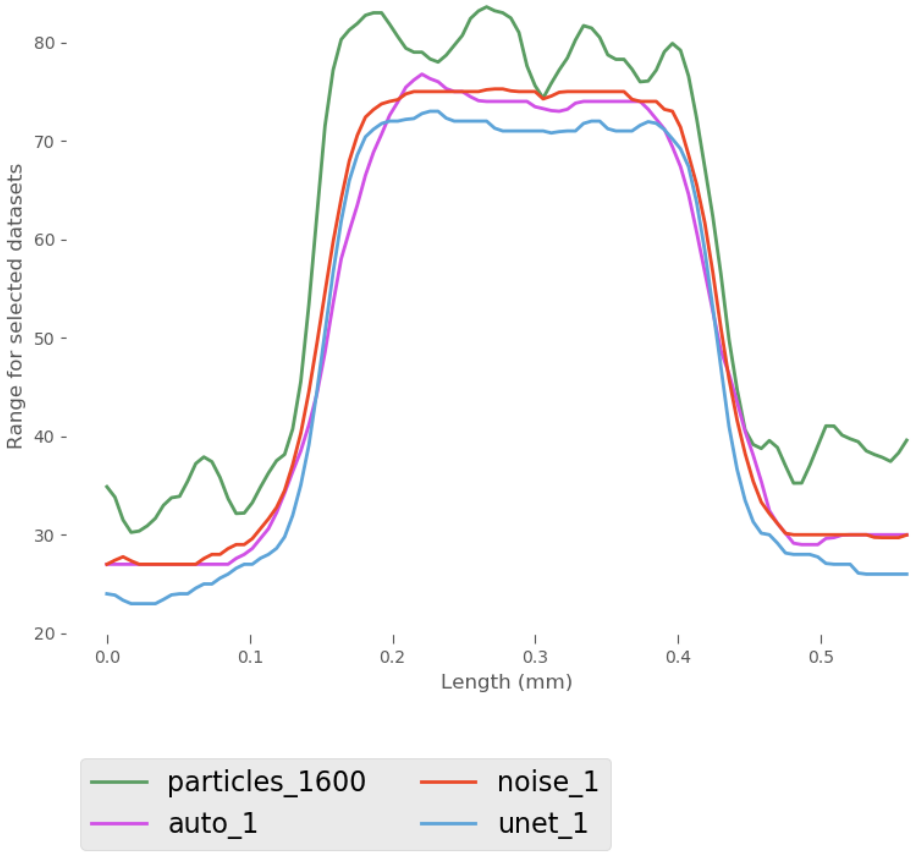

Figure 42. *Line intensity profiles for the network architecture testing. Original 1600 projection reconstruction (green), 800 projection enhancement with auto-encoder (purple), 800 projection enhancement with noise2noise (red), and 800 projection enhancement with u-net (blue).*

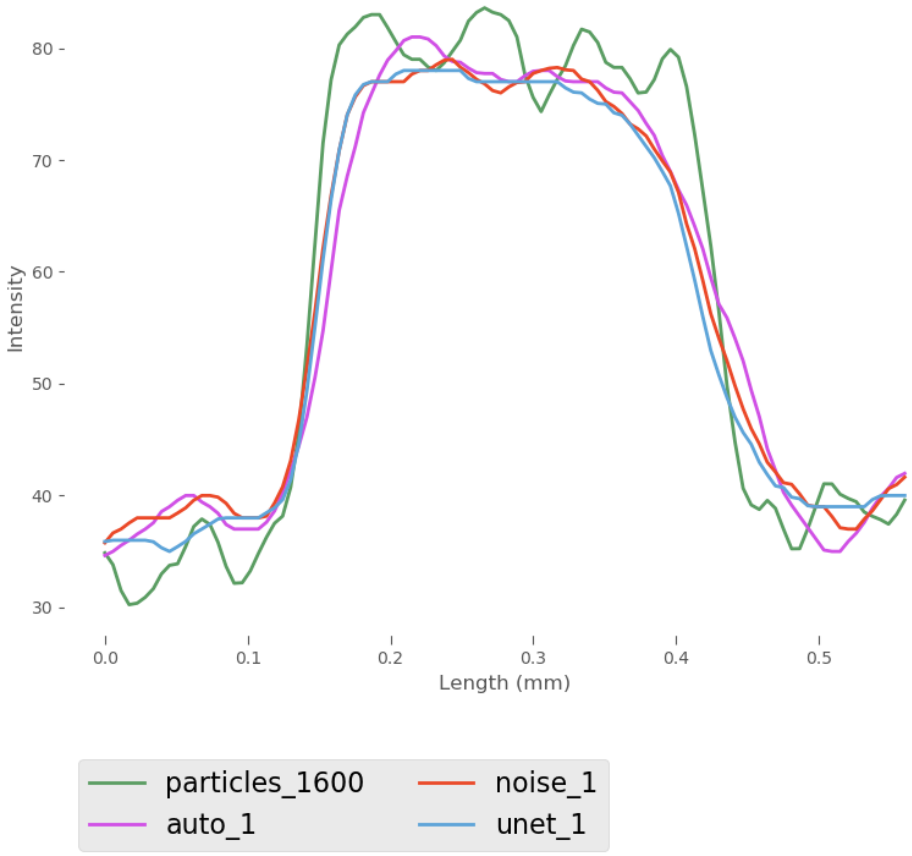

Figure 43. *Line intensity profiles for the network architecture testing. Original 1600 projection reconstruction (green), 200 projection enhancement with auto-encoder (purple), 200 projection enhancement with noise2noise (red), and 200 projection enhancement with u-net (blue).*

APPENDIX E: OUTPUT QUALITY LINE INTENSITIES

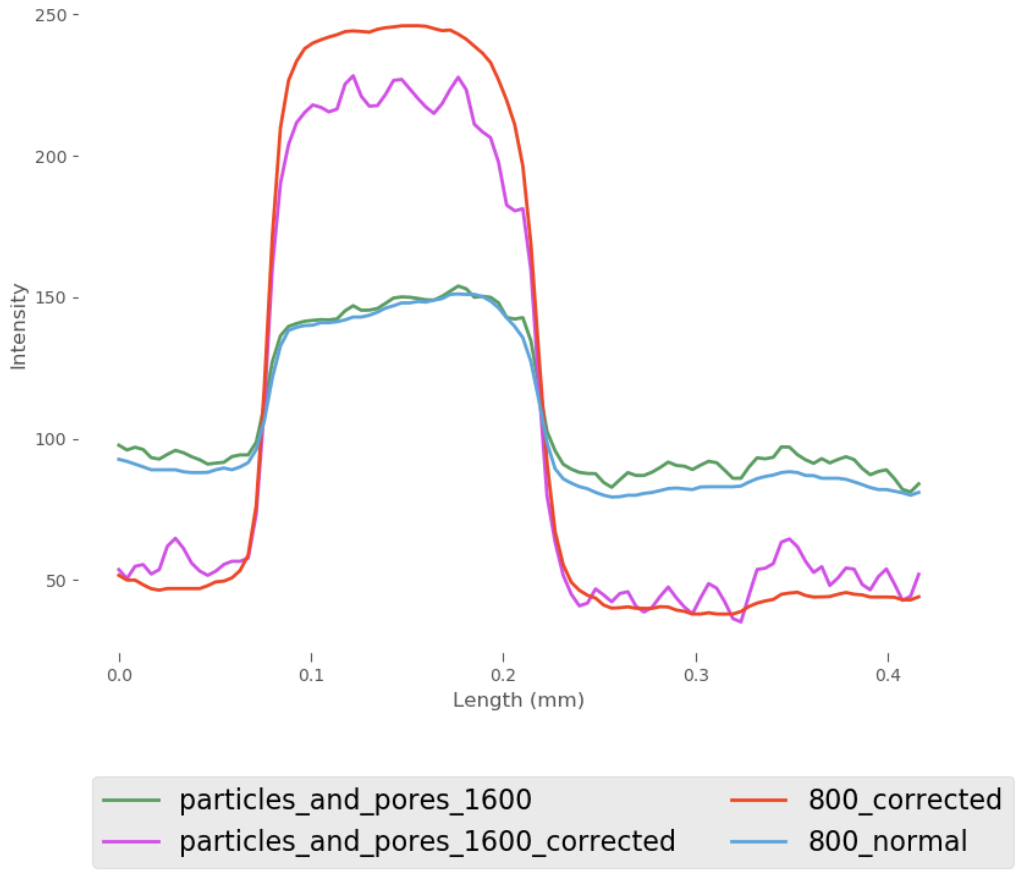

Figure 44. *Line intensity profiles for the network output quality testing. Original 1600 projection reconstruction (green), 1600 projection corrected version (pink), 800 projection enhancement (red), and 800 projection enhancement with corrected version (blue).*

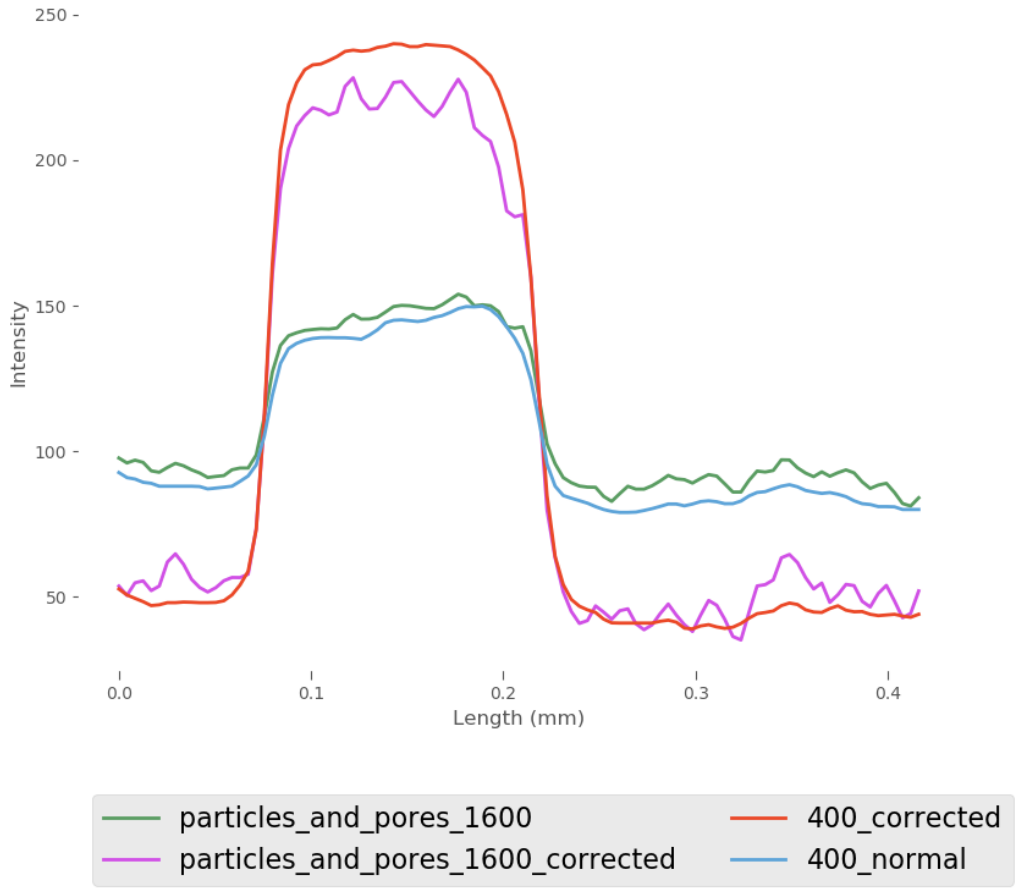

Figure 45. *Line intensity profiles for the network output quality testing. Original 1600 projection reconstruction (green), 1600 projection corrected version (pink), 400 projection enhancement (red), and 400 projection enhancement with corrected version (blue).*

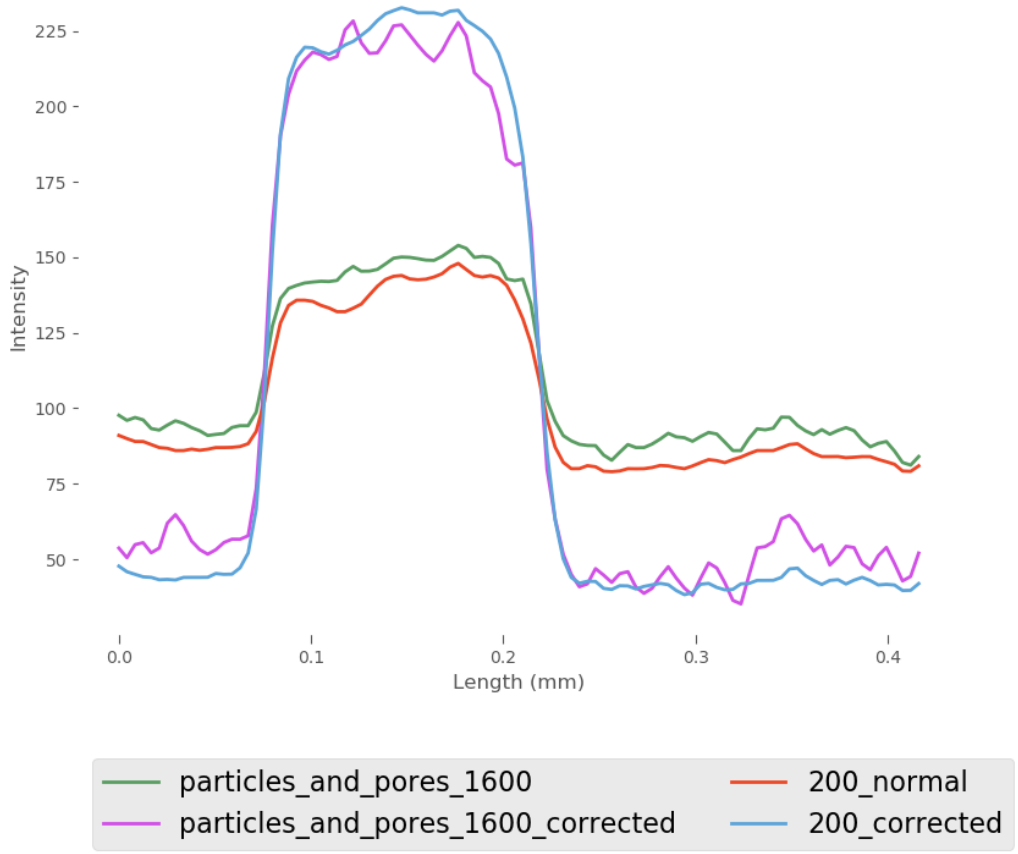

Figure 46. *Line intensity profiles for the network output quality testing. Original 1600 projection reconstruction (green), 1600 projection corrected version (pink), 200 projection enhancement (red), and 200 projection enhancement with corrected version (blue).*

APPENDIX F: PHOTON COUNT AND EXPOSURE TIME LINE INTESITIES

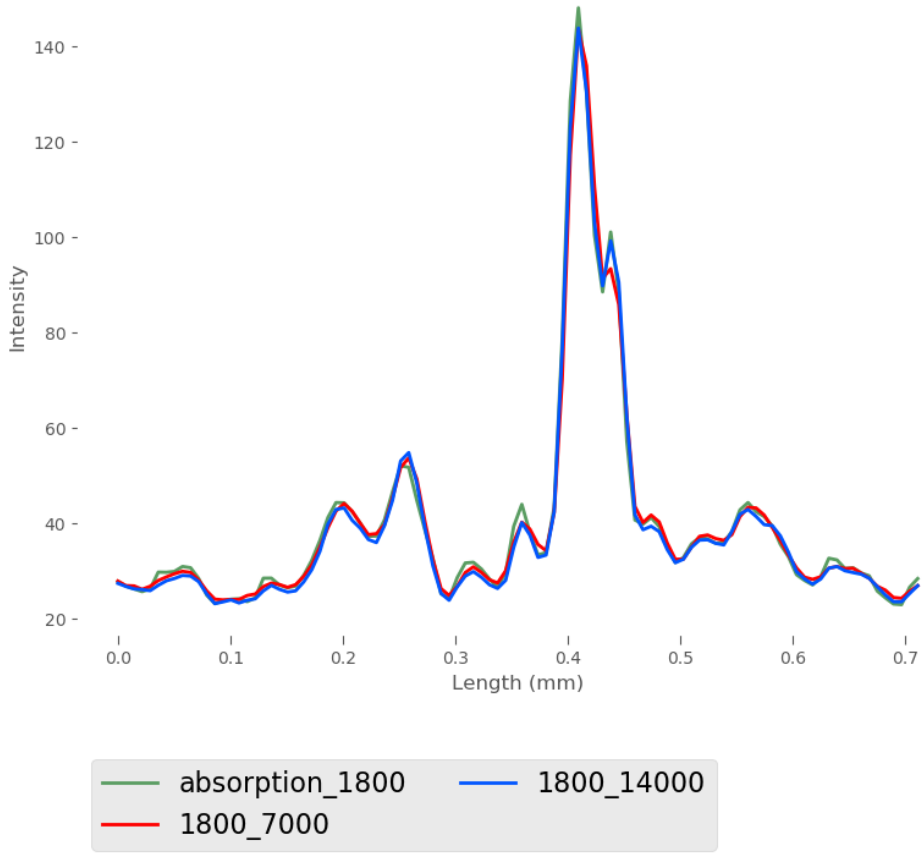

Figure 47. *Line intensity profiles for the photon count testing. Original 1800 photon reconstruction (green), 1800 photon reconstruction enhanced with network 28 (red), and 1800 photon reconstruction enhanced with network 29 (blue).*

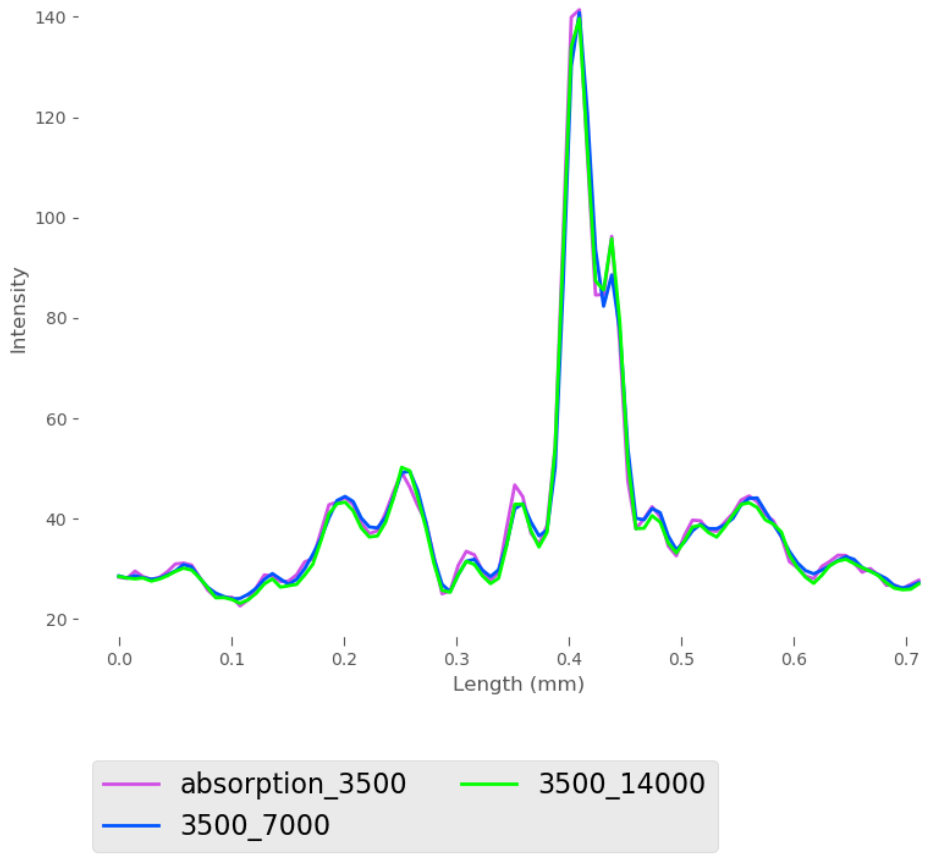

Figure 48. *Line intensity profiles for the photon count testing. Original 3500 photon reconstruction (purple), 3500 photon reconstruction enhanced with network 28 (blue), and 3500 photon reconstruction enhanced with network 29 (green).*

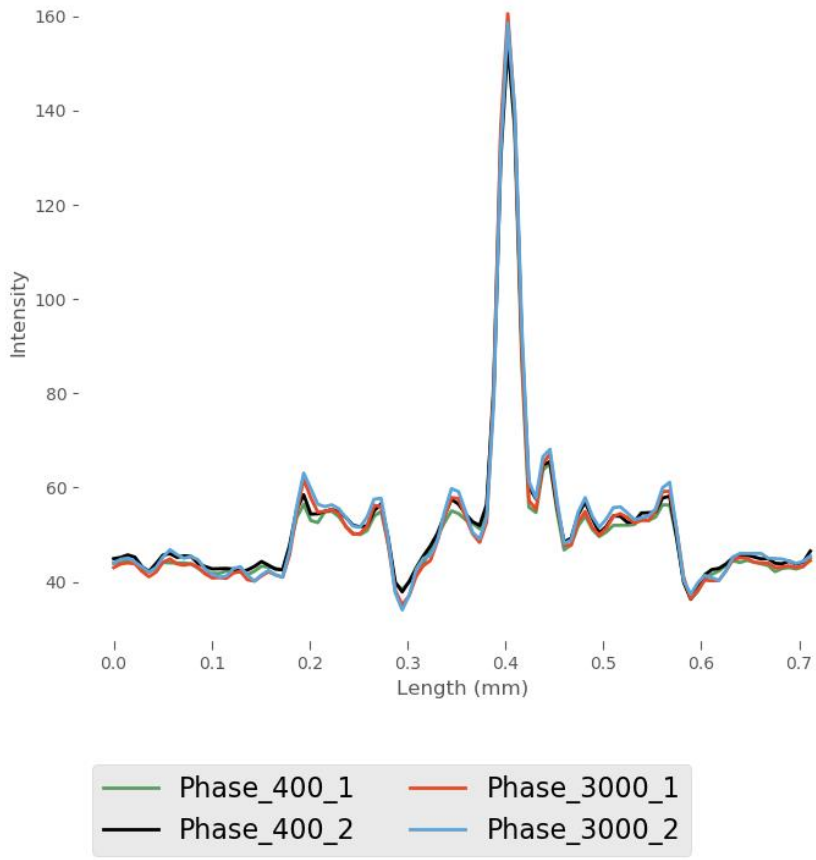

Figure 49. *Line intensity profiles for the photon count testing. 400 photon reconstruction enhanced with network 30 (green), 400 photon reconstruction enhanced with network 31 (black), 3000 photon reconstruction enhanced with network 30 (red), and 3000 photon reconstruction enhanced with network 31 (blue).*